1997

Mixing of a passive scalar in magnetically forced two-dimensional turbulence

Benjamin S. Williams

D. Marteau

Jerry P. Gollub
Haverford College

AIP | Physics of Fluids

Mixing of a passive scalar in magnetically forced two-dimensional turbulence

Benjamin S. Williams, D. Marteau, and J. P. Gollub

Citation: Phys. Fluids **9**, 2061 (1997); doi: 10.1063/1.869326
View online: http://dx.doi.org/10.1063/1.869326
View Table of Contents: http://pof.aip.org/resource/1/PHFLE6/v9/i7
Published by the American Institute of Physics.

Mixing of a passive scalar in magnetically forced two-dimensional turbulence

Benjamin S. Williams, D. Marteau, and J. P. Gollub[a)]
Department of Physics, Haverford College, Haverford, Pennsylvania 19041
and Department of Physics, University of Pennsylvania, Philadelphia, Pennsylvania 19104

(Received 13 August 1996; accepted 18 February 1997)

More than 35 years ago, Batchelor discussed from a theoretical point of view the spatial power spectrum $E_\theta(k)$ of a weakly diffusing impurity mixed by a turbulent fluid flow. Under plausible assumptions including the random straining of fluid elements, $E_\theta(k)$ is expected to scale as k^{-1} for a range of wave numbers k beyond the cutoff of the energy spectrum, followed by a diffusive tail at a wave number determined by the rate of strain and the diffusivity. Some experiments over the years appear to support this conclusion, while others do not. We have investigated this issue experimentally in a quasi-two-dimensional turbulent flow, established in a thin buoyant layer that is electromagnetically forced by an array of permanent magnets beneath the cell. The wave number cutoff of the velocity field is established by particle image velocimetry, and the fluctuations are determined to be homogeneous and isotropic. To study mixing, a dye solution is introduced steadily at one side of the buoyant layer, and mixed fluid is extracted at the other until the fluctuations become steady. The time-averaged spatial power spectrum of the dye concentration distribution is measured for several distinct forcing configurations, including both regular and random magnet arrays; the latter produces convincingly isotropic concentration fluctuations. We find that $E_\theta(k)$ falls strongly below k^{-1} at wave numbers lower than expected from theory. The results do not appear to depend significantly on the scalar injection parameters or on the magnet arrangement. Periodic forcing at higher viscosity leads to chaotic rather than turbulent flows, with little change in $E_\theta(k)$. The observations can be explained in part by the intermittency characteristic of these two-dimensional flows, where the stretching of fluid elements is localized in space and time. [S1070-6631(97)03306-0]

I. INTRODUCTION

When a weakly diffusing passive impurity is introduced into a turbulent fluid, regions of high concentration are stretched and folded repeatedly. This process creates thin striations with large concentration gradients. The large gradients enhance diffusion, so that uniformity is achieved at the smallest scales. If the source of impurity is continuous so that a steady-state situation can be achieved, then spectral analysis is an appropriate method for characterizing the mixing process. More than 30 yr ago, Batchelor[1] considered this problem in detail, and concluded that the power spectrum of the impurity should show a region proportional to k^{-1} at wave numbers higher than k_K, the inverse of the Kolmogorov scale, but smaller than a diffusive wave number cutoff that is generally called the Batchelor wave number k_B. This interval is called the viscous-convective wave number range.

In part because of the importance of mixing in many applications of fluid dynamics, e.g. in oceanography and atmospheric science, many investigators have explored the spectral properties of advected impurities experimentally[2–6] and numerically;[7–10] we review these contributions in Sec. II D. However, the various investigations are not consistent with each other with regard to the observations of k^{-1} scaling in the viscous-convective range. In this paper, we present an experimental study of the spectrum of passive scalar mixing for a two-dimensional turbulent flow. We focus on the case of a weakly diffusing impurity (a fluorescent dye) for which the Batchelor regime is expected to be well defined. This case corresponds to high Schmidt number ($\mathrm{Sc} = \nu/\kappa$, where ν is the kinematic viscosity of the fluid and κ is the diffusivity of the scalar). The flow is driven electromagnetically using a current and static magnetic fields.

The two-dimensional situation is advantageous in that the entire flow can be imaged simultaneously with video methods. This allows direct computation of spatial power spectra, as opposed to other experimental arrangements that require single-point temporal measurements. In addition, the velocity field can be measured using particle image velocimetry, so that the intimate connections between the concentration and velocity fields can be explored.

The results of this investigation reveal strong deviations from Batchelor scaling; the scalar spectrum falls strongly below k^{-1} at wave numbers lower than expected. A considerable effort has been devoted to exploring the possible reasons for this behavior. Many potential experimental explanations have been eliminated (nonlinearity of the dye; lack of stationarity or homogeneity; anisotropy; etc.). Residual three-dimensionality is a concern, but taken alone seems insufficient to account for the results. Several different forcing methods have been used to vary both the spatial and temporal properties of the velocity field, and the results are robust. We argue that the localization and intermittency of the

[a)]Corresponding author. Please use the Haverford postal address or electronic mail: jgollub@haverford.edu

strongly straining regions in these two-dimensional flows can largely account for the early spectral falloff.

In Sec. II, we give the background of the experiment, including the definitions of the measured quantities. The methods used to create the magnetically forced flows and to determine their velocity and concentration fields are given in Sec. III. The measured statistical properties of these fields are presented in Sec. IV, followed by a discussion of the work and its implications in Sec. V.

II. BACKGROUND

A. Definition of spectral functions

We first review the notation and definitions that are needed to describe the theory and present the experimental results. The transport of a scalar field $\theta(\mathbf{x},t)$ by a velocity field $\mathbf{u}(\mathbf{x},t)$ is presumed to be governed by the advection-diffusion equation:

$$\frac{\partial \theta}{\partial t} = \mathbf{u}\cdot\boldsymbol{\nabla}\theta = \kappa\ \nabla^2\theta, \tag{1}$$

where κ is the diffusivity of the scalar quantity [dimensions $(\text{length})^2(\text{time})^{-1}$]. For passive scalar fields, $\mathbf{u}$ is unaffected by θ.

The two-dimensional power spectrum $\Delta(\mathbf{k})$ of the scalar field is defined as

$$\Delta(\mathbf{k}) = \left(\frac{2\pi}{a}\right)^2 |\Theta(\mathbf{k})|^2, \tag{2}$$

where $\Theta(\mathbf{k})$ is the Fourier transform of the scalar field $\theta(\mathbf{x})$, and a is the size of the field of view. We assume that the scalar distribution is in a statistical steady state and therefore time dependence from $\Delta(\mathbf{k})$. (We discuss how we suppress the time dependence experimentally in Sec. III B and in Appendix A.) If we assume that the dye distribution is statistically homogeneous and isotropic, $\Delta(\mathbf{k}) = \Delta(k)$. It is then useful to define a further spectral function $E_\theta(k)$, which is the circular average of the two-dimensional power spectrum $\Delta(\mathbf{k})$, multiplied by a factor $2\pi k$,

$$E_\theta(k) = 2\pi k\Delta(k) = \int_0^{2\pi} \Delta(k,\phi) k\ d\phi. \tag{3}$$

Then if $\langle\theta\rangle_x = 0$ (or is forced to vanish by subtraction in the analysis) the one-dimensional integral of $E_\theta(k)$ over k is the variance of the fluctuations of θ:

$$\langle(\delta\theta)^2\rangle_x = \int_0^\infty E_\theta(k)dk. \tag{4}$$

The energy spectrum $E(k)$ gives the spectral distribution of the velocity fluctuations. If $U_n(\mathbf{k})$ is the Fourier transform of $u_n(\mathbf{x})$, where the subscript n indicates either the x or y velocity component, then $E(k)$ (for two-dimensional turbulence) is given by

$$E(k) = \left(\frac{2\pi}{a}\right)^2 \int_0^{2\pi} |U_n(k,\phi)|^2 k\ d\phi. \tag{5}$$

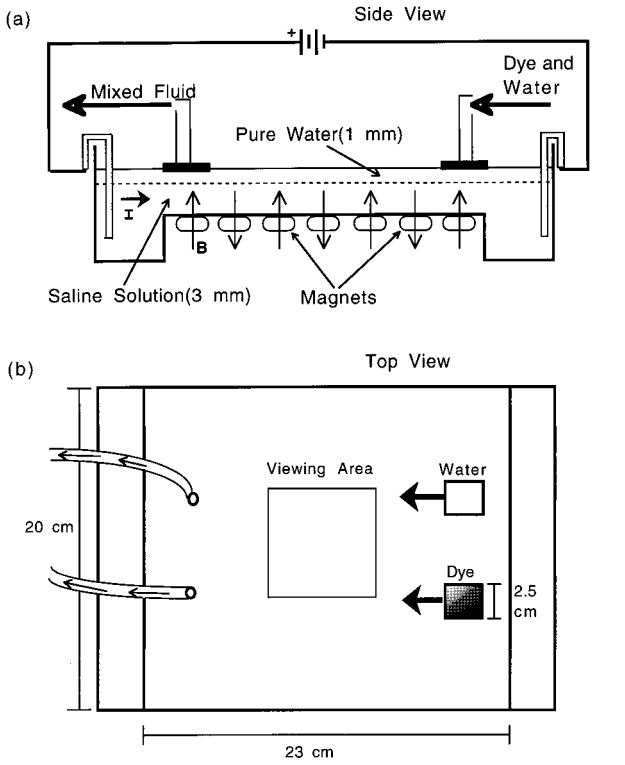

FIG. 1. Two-dimensional mixing apparatus. A thin layer of pure water lies above a layer of saline solution. Magnets mounted under the cell produce a spatially periodic magnetic field. Vortices result when a current is passed through the fluid. Dye and water are pumped slowly into sponges on one side of the apparatus and are extracted from the other side. The troughs at either end collect the heavy impurities resulting from the reactions occurring at the electrodes. (a) Side view. (b) Top view.

We use the energy spectrum only to obtain a wave-number cutoff. Since the velocity fluctuations are assumed and measured to be isotropic, $E(k)$ does not depend on which velocity component is selected.

B. Batchelor's model (and related theory) on mixing at high Schmidt number

We review Batchelor's model[1] of scalar mixing at high Schmidt number in order to state the assumptions clearly. We consider the special case of two dimensions in Sec. II C. It is assumed that the turbulence is statistically homogeneous, isotropic, and in a steady state. However, a large Reynolds number is believed not to be necessary, as pointed out originally and as emphasized recently by Holzer and Siggia.[7]

The wave number range of primary interest lies above the Kolmogorov wavenumber k_K. Over scales in this range the velocity varies linearly with position for displacements smaller than k_K^{-1}. The momentum diffuses more rapidly than the scalar, and velocity fluctuations are dissipated at smaller wave numbers than scalar fluctuations. Batchelor defined a wave number analogous to k_K that we now call $k_\mathrm{B} = (\epsilon/\nu\kappa^2)^{1/4}$ beyond which the diffusion of the scalar predominates over its advective transport. The wave numbers $k < k_\mathrm{B}$ are known as the convective range for the scalar, and the wave numbers $k > k_\mathrm{B}$ constitute the diffusive range for

the scalar. Note that the two characteristic wave numbers are related by $k_B = (Sc)^{1/2} k_K$.

We focus on the so-called viscous-convective range (Fig. 1), $k_K < k < k_B$, where momentum diffuses, but the scalar is advected. In Batchelor's model, scalar fluctuations are steadily injected into the turbulence at a large length scale L. The velocity field stretches and folds the scalar, creating components of ever higher wave number in Fourier space, until the wave number k_B is reached, where the effect of diffusion becomes significant. Here, the spectral power in a unit volume of fluid is destroyed at the mean rate $\chi = 2\kappa\langle(\nabla\theta)^2\rangle$.

Batchelor noted that the interaction of the scalar with the velocity field [given by the second term in Eq. (1)] does not change the total variance. Hence, a steady state is anticipated where the spectrum [and hence the total power given in Eq. (4)] is constant in time, but scalar variance is moving past any wave number k at rate χ. Power is injected at $k = L^{-1}$, transferred from low k to high k, and dissipated at $k = k_B$.

Next, the velocity field $\mathbf{u}(\mathbf{x},t)$ is modeled for scales in the viscous-convective range as a *uniform* straining motion with negligible rotation over the time required to compress the scalar filaments to the scale $1/k_B$. Therefore, the principal rates of strain are considered to be approximately constant in time. Batchelor solved the scalar transport equation (1), following the evolution of a typical Fourier component of θ through its interaction with $\mathbf{u}$. Assuming a steady state and using dimensional analysis to evaluate an overall constant of proportionality, he predicted that the spectrum for $k > k_K$ is

$$E_\theta(k) = -\frac{\chi}{\gamma k}\exp\left(\frac{\kappa k^2}{\gamma}\right), \quad \text{with} \quad \gamma \approx -0.5\left(\frac{\epsilon}{\nu}\right)^{1/2}. \tag{6}$$

The parameter γ is the mean value for the most negative principal strain rate, i.e., the principal strain rate responsible for the compression of filaments of the scalar, and ϵ is the energy dissipation rate. In the viscous-convective range the exponential is expected to be approximately unity, so

$$E_\theta(k) \approx -\frac{\chi}{\gamma k}, \quad \text{for } k_K < k < k_B. \tag{7}$$

Since the principal rates of strain are not constant over the entire flow, an average value must be used for γ. Batchelor also pointed out that the time required to establish such a spectrum is roughly $-\gamma^{-1}\log(\nu/\kappa)$, and hence becomes long at high Schmidt number. Dimotakis and Miller[11] have discussed the high Schmidt number limit theoretically.

Kraichnan[12] later considered the effect of temporal (and spatial) fluctuations in the rate of strain from its average value. Fluctuations were found to have little effect on the spectral shape at low k, but the diffusive tail for $k > k_B$ becomes somewhat more gradual than indicated in (6), and is expected to be exponential rather than Gaussian. In the presence of strong intermittency of the strain rate, Kraichnan's discussion implies that the spectral shape can be significantly affected.

C. Mixing in two dimensions

In this work, we study scalar spectra in two-dimensional turbulence. Although the arguments for k^{-1} scaling were initially presented in the context of three-dimensional turbulence, they are expected to hold equally well in two dimensions. However, the behavior of the energy spectrum $E(k)$ in the inertial wave number range differs from the three-dimensional $k^{-5/3}$ scaling behavior because of the conservation of vorticity. The exact dependence is unimportant for our purposes (and in any case would not apply accurately to our experiment). There still exists a cutoff wave number above which velocity fluctuations are suppressed through viscous energy dissipation. We refer to viscous cutoff by the symbol k_c and continue to refer to the diffusive cutoff as k_B. The existence of a viscous-convective range for $Sc \gg 1$ does not depend on a particular form for $E(k)$ in the inertial range, as long as the velocity field consists of a random straining motion on small scales. With this form for the velocity field $\mathbf{u}$, Batchelor's conclusion that $E_\theta(k) \propto k^{-1}$ for $k_c < k < k_B$ is generally assumed to be valid in two dimensions. However, the assumption of a random straining field may be more difficult to justify when there are coherent long-lived vortices. On the other hand, Vulpiani[13] has argued that the k^{-1} scaling in two dimensions should be more general than in three dimensions, extending to wave numbers in the inertial range, and applying even for chaotic advection with few degrees of freedom.

D. Previous experimental and numerical work

1. Experiments

The experimental evidence supporting the existence of a k^{-1} spectrum has been inconclusive. Gibson and Schwarz[2] studied both temperature and salinity ($Sc \approx 700$) fluctuations in water made turbulent by passing it through a grid. The slope of the scalar spectrum was found to be less negative at wave numbers above than below the velocity cutoff, and they concluded that the data were consistent with Batchelor's predictions. However, the scatter is large and the scaling range is limited. Grant *et al.*[3] simultaneously measured temperature and velocity fluctuations in the ocean ($Sc \approx 7$). The scalar spectrum was seen to change from $k^{-5/3}$ to approximately k^{-1} in the region of the velocity spectrum cutoff. This k^{-1} scaling was seen over a decade of wave numbers, a greater range than one might expect for a Prandtl number of 7. However, Grant *et al.* thought it likely that the turbulence was not locally isotropic, as required by the Batchelor theory. Nye and Brodkey[5] mixed dye with water ($Sc \approx 5000$) in pipe turbulence and found a full 1.5 decades of k^{-1} behavior, starting near the velocity spectrum cutoff, which was observed to be at about $0.1k_K$. Gargett[14] measured temperature and velocity spectra in both isotropic and anisotropic oceanic turbulence. Batchelor scaling was not observed for the isotropic case. However, the slope of $\log E_\theta(k)$ was close to -1 when the velocity field was anisotropic as a result of buoyancy. Gibson later commented on the important role of intermittency in oceanic measurements.[15]

More recently, Wu *et al.*[6] argued that the thickness fluctuations of a soap film act as a passive scalar under certain limiting conditions. They used a two-dimensional eccentric Couette cell to create turbulence ($\mathrm{Re} \approx 8000$) in a stretched film. They noted well-defined k^{-1} scaling [though they omitted the phase space factor in (3), so that their plotted spectra varied as k^{-2}]. The properties of the velocity field were not measured in this experiment. Since thickness variations exert an elastic force on the film, the accuracy of the approximation that thickness fluctuations behave as a passive scalar is difficult to assess.

Miller and Dimotakis[4,16] performed careful experiments on dye mixing in water ($\mathrm{Sc} \approx 2000$) in a turbulent jet ($12\,000 < \mathrm{Re} < 72\,000$). They gave particular attention to experimental issues that could affect the data at high wave numbers. The spectrum $E_\theta(k)$ did not follow a power law, and was generally steeper than k^{-1} in the (expected) Batchelor regime. They pointed out that some of the previous positive reports had inadequate spatial resolution or too low a Schmidt number to make a proper test.

2. Simulations

Holzer and Siggia[7] performed two-dimensional numerical simulations. They solved a stochastically forced Euler model in Fourier space within a limited band of wavenumbers. At high Sc the diffusion of the scalar takes place at wave numbers beyond the forcing band. To maximize the range of scales available, hyperdiffusivity was used. The computations were consistent with Batchelor scaling.

Antonsen *et al.* used an eikonal-type reduced wave number description instead of the full transport equation (1) to simulate the interaction of the velocity field and the scalar in two dimensions. A Lagrangian chaotic flow was used as the forcing field. They obtained k^{-1} scaling both for their reduced equations, and for the full advection-diffusion equation in spectral space, for their chosen forcing field. However, the results may be relevant primarily to Schmidt numbers much higher than those that occur in realistic experiments.

Pierrehumbert[10] simulated mixing using a two-dimensional (2-D) chaotic mapping designed to simulate a large-scale 2-D velocity field. The chaotic mapping alternates with a diffusive smoothing step in this computation. There were a number of interesting and relevant results: (a) For a decaying scalar field that is not resupplied, the concentration spectrum at a given time is exponential rather than algebraic. (b) For steady-state mixing with injection at large scales, spectra are algebraic, but with anomalously steep exponents between -1 and -2. Furthermore, the scalar probability distribution shows a substantial amount of ''mixed'' fluid with intensities between the maximal and minimal values. (c) The power spectra approach k^{-1} only if an exceptionally wide scale separation between the viscous and diffusive scales is maintained. These results suggest that k^{-1} scaling may not be robust in 2-D experiments at physically realistic Schmidt numbers.

Direct numerical simulations for high Schmidt number three-dimensional turbulence are difficult to perform because of the large range of scales relevant to the mixing. This requires that simulations be implemented at very high resolution, so the computations are demanding. Bogucki, Domaradzki, and Yeung[8] performed a three-dimensional direct numerical simulation in spectral space, with Taylor microscale Reynolds numbers of 25, 36, and 77, using resolutions of 162^3, 162^3, and 240^3, respectively. They observed k^{-1} scaling over more than a decade of wave numbers, even for relatively low Schmidt numbers $\mathrm{Sc} = 3$, 5, and 7. Much of this scaling range was located at wave numbers lower than the traditional estimates, where the energy spectrum has substantial power [but the scalar dissipation $k^2 E_\theta(k)$ is fairly small]. An exponential tail consistent with Kraichnan's form was found.

III. METHODOLOGY

A. Two-dimensional flow cell

A combination of electromagnetic forcing and density stratification is used to create a quasi-two-dimensional flow. The cell, based on a design by Cardoso, Marteau, and Tabeling,[17] is shown in Fig. 1. It is an open rectangular container made from Delrin, with a thin (1 mm) glass bottom. A glass window mounted in the side of the cell permits lateral visual inspection of the flow. A 3 mm layer of saline solution (NaCl and water, 3.2 M) is placed in the cell. A spatially periodic magnetic field is created by permanent magnets placed beneath the glass bottom. The flow is driven by passing a steady current through the saline solution. The magnetic field exerts a force on the moving charges perpendicular to their velocity and the magnetic field. The forcing current can be either constant or time periodic. In the latter case, chaotic advection occurs; this allows mixing to be studied at lower Reynolds numbers and hence higher viscosities.

Several different arrangements of magnets are used in these experiments. Figure 2(a) shows a regular array yielding unstable shear zones that evolve to an irregular array of vortices with typical spacing of several cm. As the current is increased, so does the speed of the flow; the vortices become unstable and move around the cell erratically. The resulting nonperiodic flow is a form of weak turbulence; its statistical properties are discussed in Sec. IV A. Some additional experiments were done with a random magnet array, as shown in Fig. 2(b). Both the coordinates and the polarizations were randomly selected; overlapping coordinate choices were simply omitted.

To study 2-D mixing, we require a thin moving layer of fluid within which the velocity field is nearly independent of depth. To achieve this, we place a 1 mm layer of fresh water above the denser (1.15 g/ml) 3 mm layer of saline solution. Buoyancy forces act to keep the layers separate over the length of an experimental run, about 10 min. As the upper layer is not electrically conductive, it is forced only through contact with the lower layer.

In our investigation the concentration of a fluorescent dye solution (sodium fluorescein) in pure water serves as the passive scalar. The diffusivity of the dye[18] is 5×10^{-6} cm^2 s^{-1}; this yields a Schmidt number $\mathrm{Sc} \approx 2000$. Fluctuations are introduced by injecting dye solution (concentration of 0.0015 M) and pure water into the upper layer

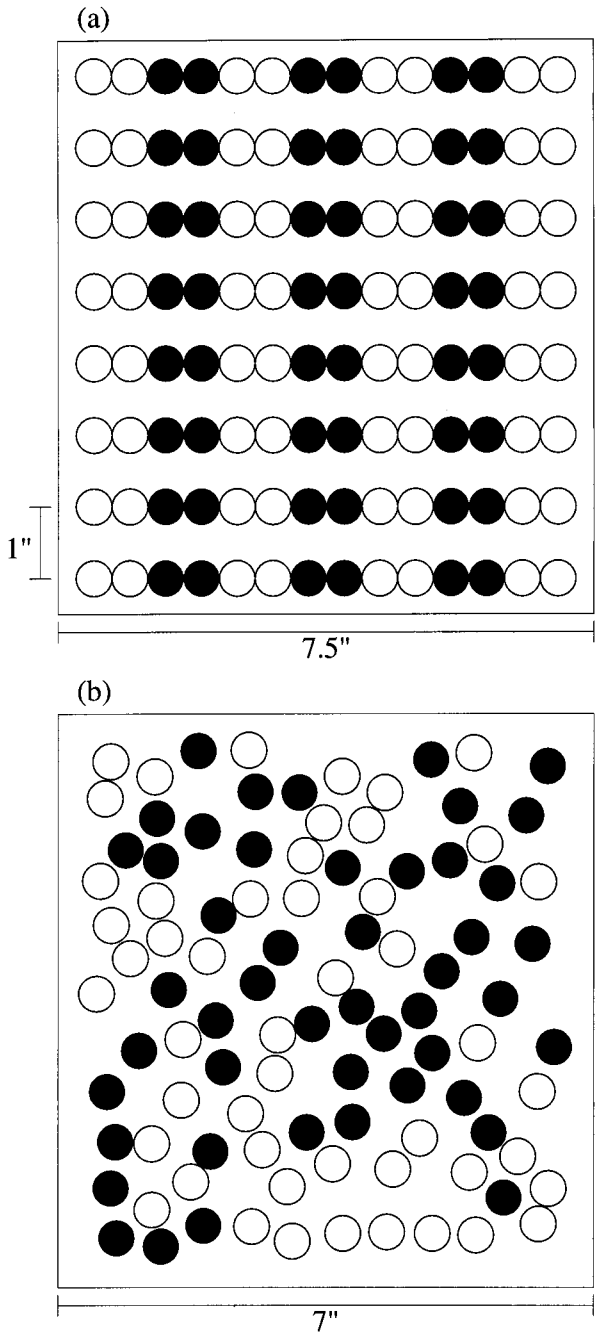

FIG. 2. Arrays of 1.25 cm diam magnets placed beneath the cell. Black and white denote the two polarities. (a) Regular array in rows separated by 2.5 cm. (b) Random arrangement (see the text).

of the flow through sponges in contact with the surface, as shown in Fig. 1(b). Injection takes place sufficiently slowly so as not to affect the dynamics of the flow. Mixed fluid is extracted (at an equal rate) from the upper layer on the opposite side of the cell. After an initial transient period, a steady state is achieved. We choose the relative injection rates of dye and water to yield the best signal-to-noise ratio.

For the flow in the upper layer to be considered two dimensional, there should be neither vertical velocity components nor vertical velocity gradients. Two effects suppress vertical velocity components. First, the magnets are placed as close as possible to the lower layer, so that the direction of

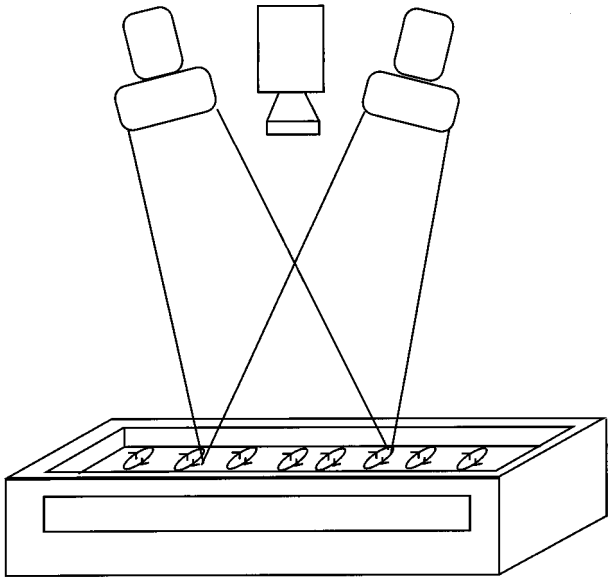

FIG. 3. Illumination and imaging setup. Illumination of the dye is provided by four horizontal low intensity UV-emitting tubes (not shown) placed on either side of the cell and two high-intensity UV lamps mounted overhead. The concentration field (or particle distribution for velocimetry) is imaged by the shuttered CCD camera. A side window allows the extent of vertical mixing to be evaluated.

B varies only slightly from the vertical throughout the 3 mm electrolyte layer. The close spacing of magnets ensures rapid transitions from regions of positive to negative **B**. As a consequence, the Lorentz forces produced in the lower layer act principally in the horizontal plane. Second, the stratification by density inhibits mass transfer between the two layers.

Vertical velocity gradients in the upper layer are created when the lower layer accelerates, pulling the upper layer along. This can have the effect of smearing thin filaments of dye. We minimized such gradients by keeping the upper layer as thin as possible. We also performed some experiments with a glycerol–water solution to reduce the vertical velocity gradients. The adequacy of the two-dimensional approximation is discussed in Appendix B.

B. Scalar measurement

We measure the concentration of the fluorescent dye by illuminating the flow with ultraviolet lamps radiating near 365 nm, as shown in Fig. 3. The incident UV intensity is nearly uniform over the imaged area. The dye concentration in the imaged area is kept below about 10^{-4} M, where the intensity is found by a separate calibration test to increase linearly with concentration to within about 10%. At higher concentrations, gradual saturation occurs.

Images of a region in the center of the flow (4.8–11 cm per side, or 6%–26% of the cell) are generally obtained at 5 s intervals (so that they are not strongly correlated). We use a 512×512 pixel, variable scan CCD camera in conjunction with a liquid crystal shutter. The exposure time of each image is adjusted to minimize blurring of the dye without sacrificing signal-to-noise ratio. Each CCD array element produces a voltage proportional to the incident intensity of light.

The images are acquired by a frame grabber and stored digitally. Each pixel in the image is assigned an eight bit value according to its intensity. An average frame recorded with the shutter closed is then subtracted from each flow image to remove the effect of CCD dark current and fixed pattern noise. The result of this process is a discretely defined two-dimensional concentration function $\theta(x_i, y_i, t_i)$.

To obtain spectra, the mean intensity is first subtracted from each image. The concentration function $\theta(k)$ is multiplied by a Hanning window and transformed using standard fast Fourier transform software. After squaring, the spectra from a temporal series of images are averaged together. We then subtract the averaged 2-D spectrum of dark images (measured separately) from the 2-D signal spectrum. This removes noise associated with the dark current of the CCD and amplifier noise. The result is a mean two-dimensional spectrum of the flow, $\Delta(\mathbf{k}, \phi)$. The one-dimensional spectral function is then obtained using Eq. (3). For a full discussion of the signal processing methods, see Appendix A.

Precise determination of the wave number below which velocity fluctuations are damped is possible only empirically, as a large part of the energy is lost through friction with the bottom of the mixing cell. However, we still expect that velocity fluctuations are suppressed above a characteristic cutoff wave number k_c. This wave number is found through examination of the energy spectrum $E(k)$ for the velocity field. We use velocity fields obtained through digital particle image velocimetry (Sec. III C) for this purpose.

We also perform tests to verify the theoretical assumptions made about the nature of the mixing and the turbulence. As explained in Sec. II B, it is usually assumed that the mixing occurs in a steady state, with the total spectral power remaining constant over time. This can be checked for our experiments by monitoring the variance $\langle(\delta\theta)^2\rangle_{\mathbf{x}}$, as it is equal to the total spectral power [Eq. (4)]. To this end, the mean concentration $\langle\theta(\mathbf{x},t)\rangle_{\mathbf{x}}$ and the standard deviation of the scalar field are computed for each image and monitored over time. Because the entire cell is not imaged, the mean concentration and standard deviation are expected to vary somewhat over short time intervals, though without long term drift.

C. Velocity measurement

In order to characterize the 2-D velocity field $\mathbf{u}$ of the flow, we perform separate digital particle image velocimetry (DPIV) experiments to obtain velocity fields for the flow at discrete points in time.

The technique for DPIV is fairly standard. For a comprehensive treatment see Willert and Gharib.[19] We seed the upper layer with fluorescent polystyrene spheres 120 μm in diameter. Their density is 1.05 g/ml, slightly higher than that of water. Because the density of the lower saline layer is 1.15 g/ml, the particles reside at the boundary between the two layers. Images are typically separated by 1/22 s. We obtain images of 512×512 pixels, and select correlation zones 32 pixels on each side. The zones are overlapped by 75% to produce a 64×64 array of velocity vectors. There would be 16×16 fully independent velocity vectors (if not overlapped).

In a typical velocity field containing 4096 vectors, we find 20–40 erroneous velocity vectors, caused by false peaks in the correlation function. False peaks are caused when particle images are truncated by the edges of the correlation zone, or else leave the zone completely between frames. These effects are minimized by seeding the particles as densely as possible, so that most particles stay in the zone during the interval Δt. Additional errors can occur if particles clump together or cannot be distinguished from one another. Any erroneous vectors can be detected by comparing them with their neighbors. If the x or y components of a velocity vector differ by more than a predetermined threshold value, the vector is removed and replaced by the average of its good neighbors. This process works best when velocity field varies slowly in space (compared to the spacing of velocity vectors). This is the reason why correlation zones are overlapped to sample the velocity field beyond the range of its theoretical frequency response.

The spatial frequency response of the DPIV process depends on the size of the correlation zone used to obtain the vector. Because the process averages the displacements of all the particles in the zone, the response is that for a box:

$$R(\mathbf{k}) = \left(\frac{\sin ck_x}{ck_x}\right)\left(\frac{\sin ck_y}{ck_y}\right), \tag{8}$$

where c is half the size of the correlation zone.

We obtain velocity fields for the same driving current used during the mixing experiments. Using these fields, the root mean square speed of the flow is obtained and the Reynolds number estimated. The mean structure of the flow is obtained by time averaging a series of velocity fields, and the pattern of fluctuations can then be obtained by subtraction. We compute the one-dimensional velocity spectrum $E(k)$ as follows. After applying a Hanning window, the x or y component of the velocity field is transformed using a two-dimensional FFT algorithm. The resulting two-dimensional power spectrum is then divided by the square of the response function $R(\mathbf{k})$ [Eq. (8)]. The function $E(k)$ given in Eq. (5) is then examined for the cutoff in the velocity spectrum.

IV. RESULTS

A. Velocity fields

We performed dye mixing runs for the regular magnet array shown in Fig. 2(a) (driven at 80 mA) as well as for the random magnet arrangement shown in Fig. 2(b) (driven at 100 mA). The regular array creates long regions of the like sign magnetic field in the y direction, and thus large shearing areas at the boundaries between these regions. The resulting shear flow is unstable and decays to moving vortices. Typical measured velocity fields are shown in Fig. 4. For the regular array (Fig. 5) the rms speed is 1.8 cm/s (averaged over space and time), with a maximum speed of approximately 3 cm/s. The diameter of a typical vortex, determined by the magnet spacing, is 5 cm, so $\mathrm{Re}\cong500$.

With the random magnet arrangement (Fig. 5) the rms speed is 1.54 cm/s. The random arrangement results in some

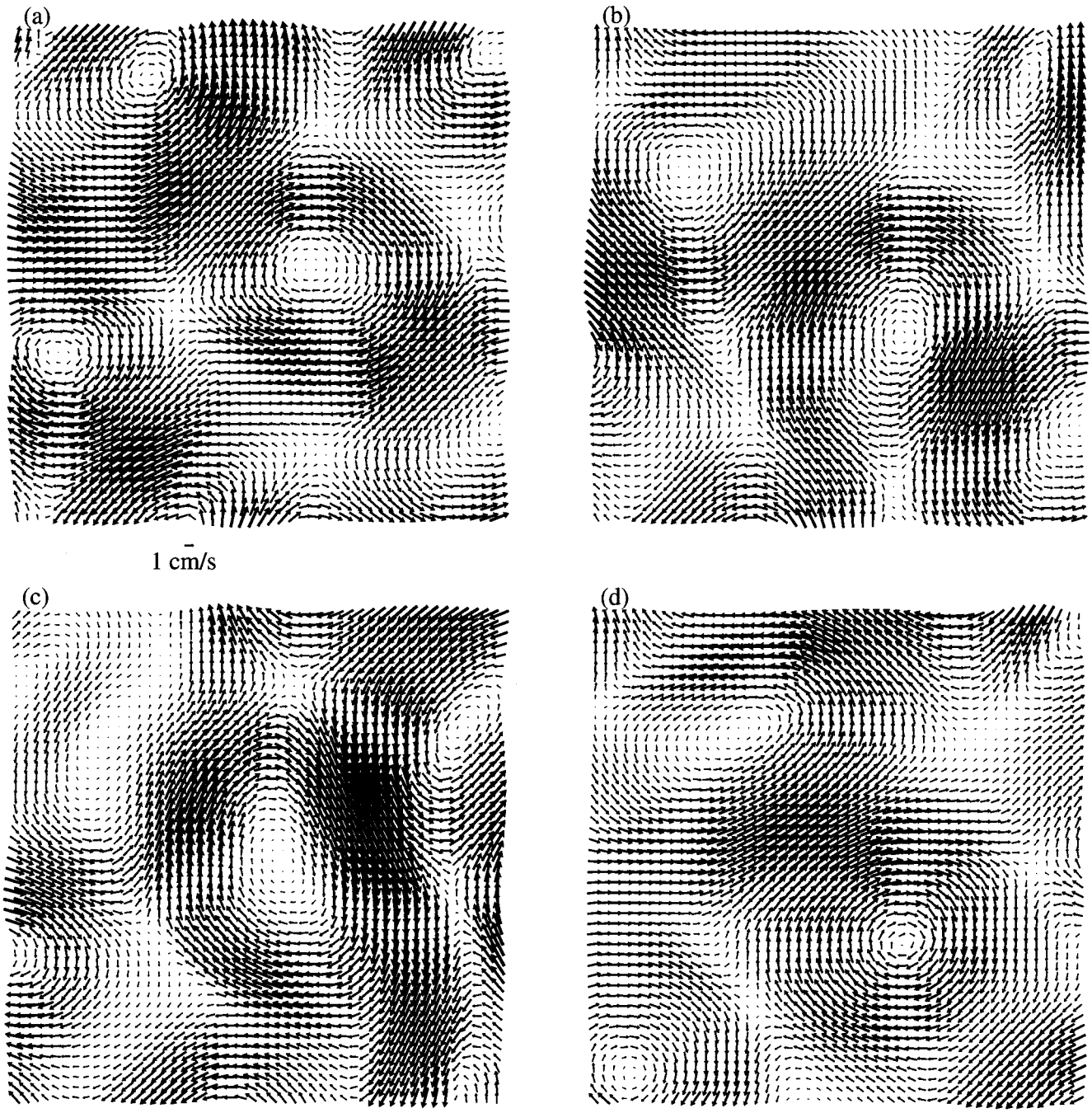

FIG. 4. Velocity fields (48×48 vectors) for the flow corresponding to the regular magnet array in Fig. 2(a). The length (and boldness) of each vector are proportional to the magnitude of the velocity at each point on the grid. Each field represents an area of 9 cm×9 cm; they were obtained at 5 s intervals.

reduction of speed and in the amount of shearing. As a result, the flow is slightly more stable. The velocity field also shows slightly sharper features in this case.

1. Homogeneity and correlation time of the velocity fluctuations

Time averaging of the velocity field reveals a definite structure imposed by the magnet array, as shown in Fig. 6. For the regular array, the mean flow varies with the same periodicity as the magnet array: 5 cm. The regions of strongest mean flow have speeds slightly over 1 cm/s, about half the rms fluctuation of the instantaneous flow. The random array also creates a mean flow, shown in Fig. 6(b). The strongest regions of mean flow in this case are roughly 1.5 cm/s, on the same order as the rms speed.

The Batchelor theory requires that in the viscous-convective range, the velocity field consists of a spatially homogeneous, random straining motion. The spatial uniformity of the fluctuations can best be judged by examining the ''standard deviation field'' for the two velocity components. This field, shown in Fig. 7 for the two arrays, is determined by plotting *at each point* the local root mean square fluctuation $(\nu_x - \overline{\nu_x})$ and similarly for ν_y, where the overbar denotes the local time average. The orientation of these vectors

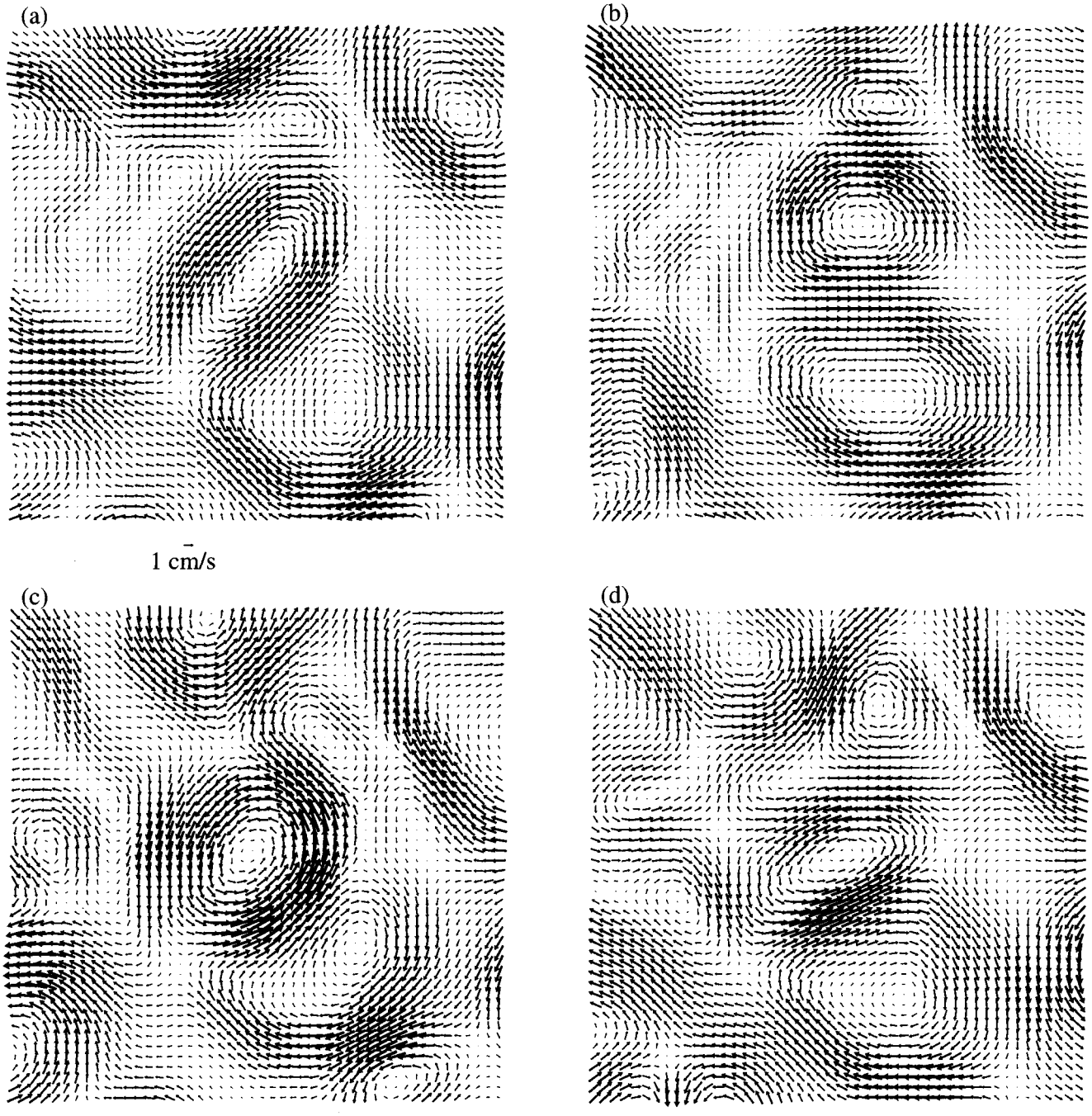

FIG. 5. Velocity fields corresponding to the random magnet arrangement in Fig. 2(b) for a steady current. The region shown is 10.2×10.2 cm.

near 45° simply means that the fluctuations of the two velocity components are approximately equal in magnitude. The spatially averaged standard deviation of v_y (0.95 cm/s) is only slightly less than that of v_x (1.11 cm/s). These fluctuations are comparable to the magnitude of the mean flow in its strongest regions. The random magnet arrangement produces somewhat smaller fluctuations about its mean flow; the spatial averages of the standard deviation of v_x and v_y are both 0.7 cm/s in this case.

The fluctuations are also approximately uniform over the imaged area. The spatial variation of the fluctuations (i.e., the standard deviation of the standard deviation field) is only about 0.15 and 0.18 cm/s, respectively, for the x and y components for the regular array. The random case is not quite as homogeneous. To summarize, we find that, although a significant mean flow exists, *the velocity fluctuations are substantial, relatively isotropic, and roughly uniform over the imaged area*.

To determine the *correlation time* of the fluctuations, we compute the temporal autocorrelation function of the velocity component fluctuations (with respect to the time-averaged mean flows of Fig. 6). This quantity is computed locally and then averaged over space. The result for the random array, shown in Fig. 8, reveals a correlation time of about 4 s, which is comparable to the eddy turnover time.

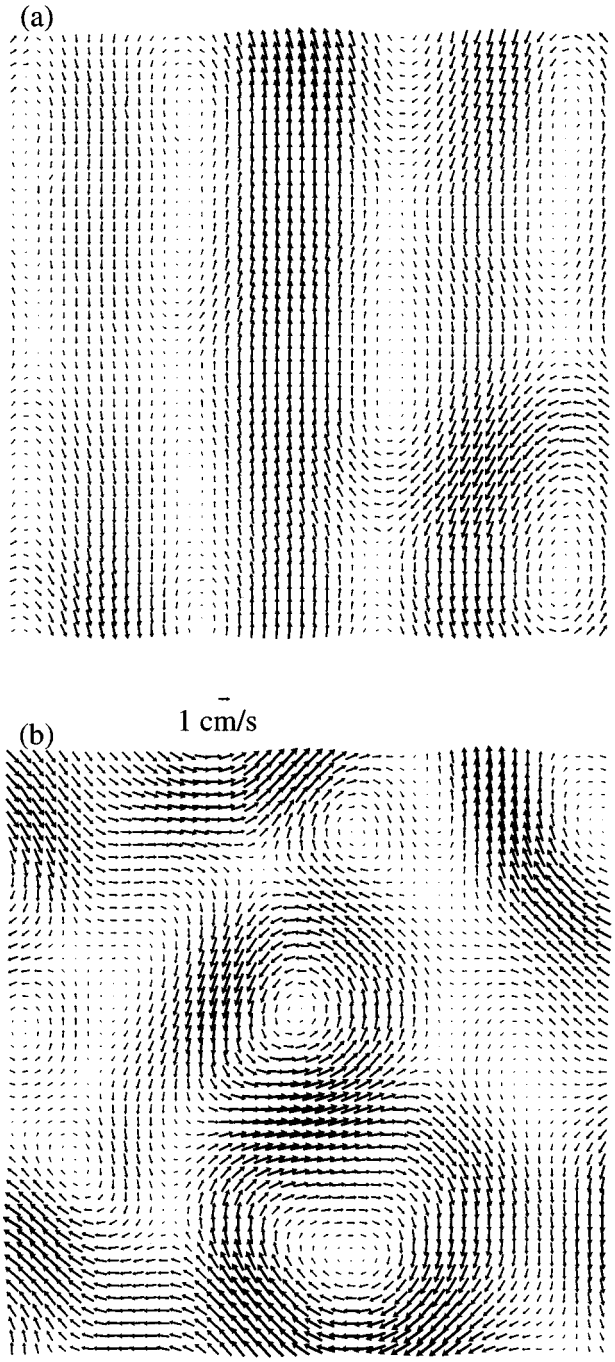

FIG. 6. Time-averaged velocity fields (mean flows) for the regular and random magnet arrangements. (a) Regular magnet array, averaged over 165 s. A mean flow with a characteristic scale of about 5 cm is present due to the magnets. (b) Random magnet array, averaged over 270 s.

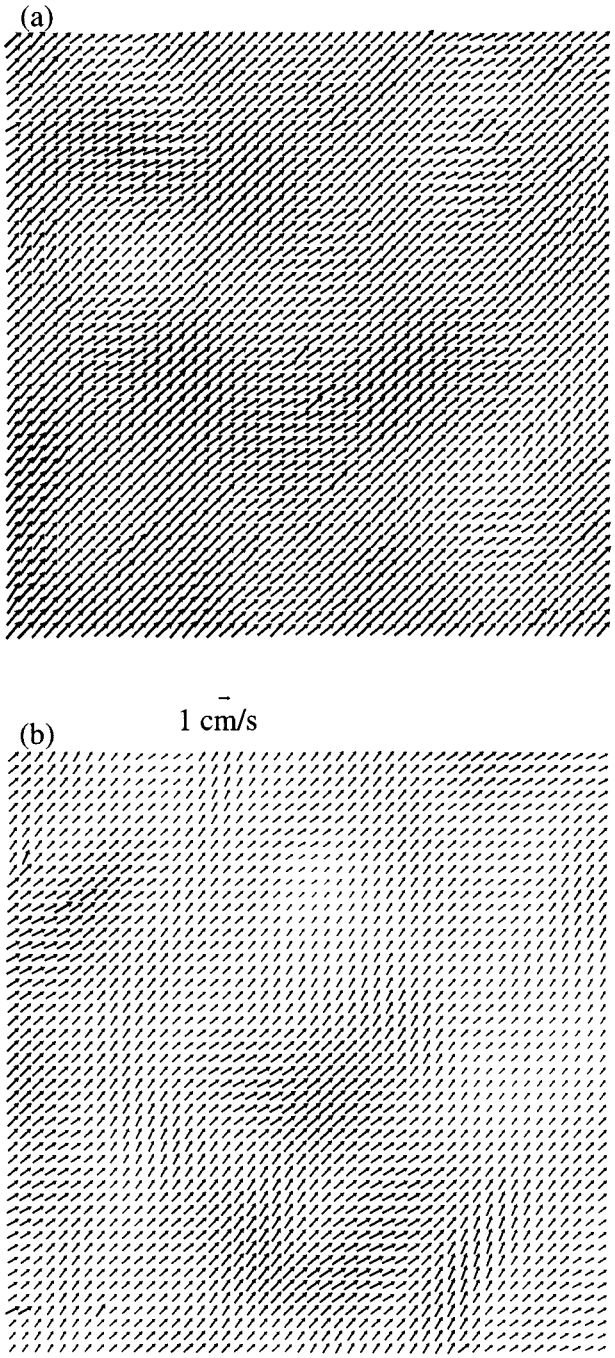

FIG. 7. Standard deviation fields for the velocity, computed with respect to the mean flows of Fig. 6. The x and y components of the vectors indicate the magnitude of the fluctuations of the x and y velocity components at each point, computed from a series of velocity fields. The direction of the vectors has no meaning, aside from giving the relative level of x and y fluctuations. (a) Regular magnet array. Fluctuations are uniformly distributed and have an average absolute magnitude of 1.4 cm/s. (b) Random magnet array. Fluctuations show more structure and have an average magnitude of 1.0 cm/s.

2. Velocity spectra: Estimating the energy cutoff

The k^{-1} scaling regime is dependent on the existence of a region of wave numbers $k_c < k < k_B$, where velocity fluctuations have been suppressed by viscosity, but scalar fluctuations have not been dissipated by diffusion. The wave number k_c is expected to be slightly different for the two magnet arrangements, as the magnetic field varies on different length scales. To determine k_c, we present velocity spectra obtained from the DPIV velocity fields in Fig. 9. Although the spectral range of $E(k)$ is limited, it is clear that for the regular magnet array the spectral power at $k/2\pi = 1\ \mathrm{cm}^{-1}$ is smaller by three orders of magnitude than at $k/2\pi = 0.2\ \mathrm{cm}^{-1}$. This is consistent with direct visual observations that there are no significant velocity fluctuations with a wavelength less than 1 cm. Therefore we choose $k_c/2\pi \cong 1\ \mathrm{cm}^{-1}$.

The spectra for the random array shown in Fig. 9(b) are

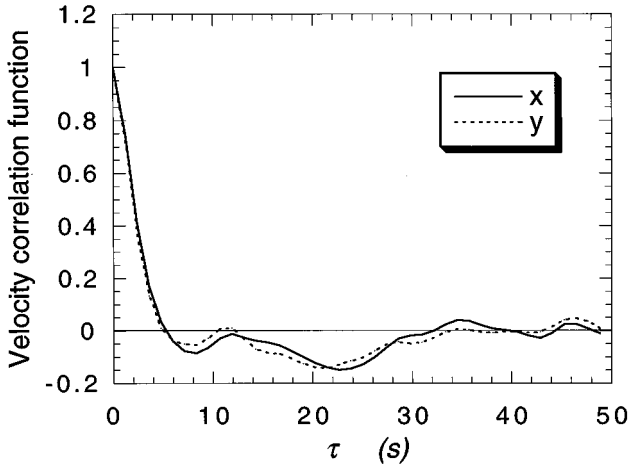

FIG. 8. Spatially averaged temporal autocorrelation functions of the velocity component fluctuations for the random array. The mean flow was first subtracted, and the temporal autocorrelation function computed at each position prior to spatial averaging.

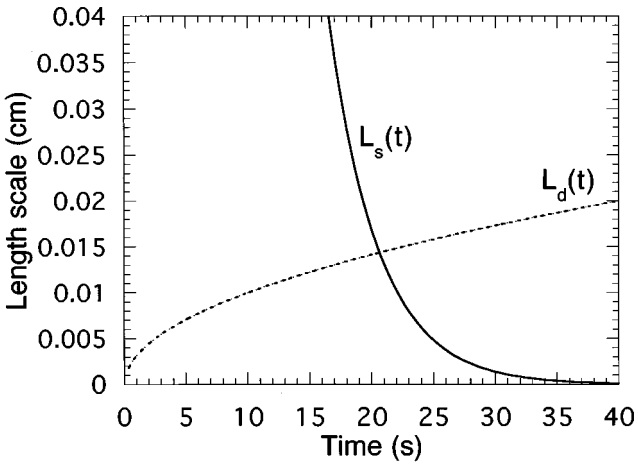

FIG. 10. Evolution in time of typical lengths due to stretching and diffusion are given by $L_s(t)$ and $L_d(t)$, respectively. The smallest and oldest structures present in the flow, i.e. those corresponding to the Batchelor wave number, should be given by the point of crossing.

qualitatively similar to those for the regular array, except that the cutoff occurs at a slightly higher wave number; we choose $k_c/2\pi \cong 1.5\ \mathrm{cm}^{-1}$ for this case. Were we instead to choose the wave number of maximum energy dissipation as k_c, the estimated viscous-convective regime would begin at wave numbers lower by a factor of 2 approximately. This situation is rather different from the usual 3-D case, where the spectral power varies more gradually near k_{K}, so that the viscous-convective regime for the scalar field can begin as low as $0.1k_{\mathrm{K}}$.

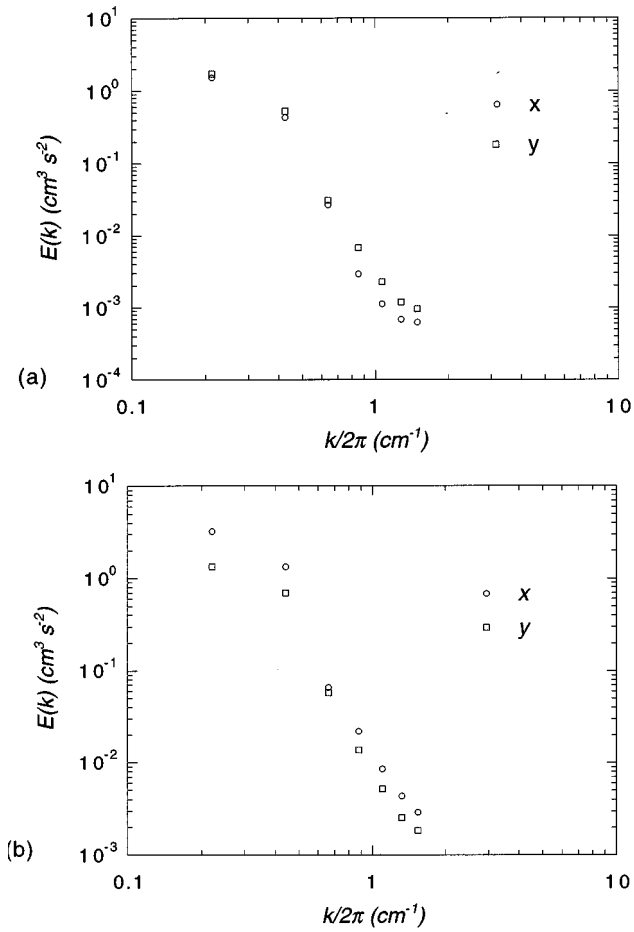

FIG. 9. One-dimensional velocity spectra $E(k)$ for the x and y components of velocity for (a) the regular array and (b) the random arrangement. Spectra are compensated for the spectral falloff caused by the finite size of the correlation zone.

3. Estimating the Batchelor wave number

We can obtain a simple physical estimate of the other end of the viscous-convective range, i.e., the location of the two-dimensional Batchelor wave number k_{B}, in several different ways. First, we consider the competing effects on a dye structure due to (a) the stretching produced by the large-scale flow and (b) the dissipation due to diffusion.[18] A dye structure of initial size L_0 is stretched once every characteristic time τ_s. This process produces an exponential decrease of its characteristic length scale. The resulting length scale is

$$L_s(t) = L_0 e^{-t/\tau_s}. \tag{9}$$

The effect of diffusion is to smooth the dye over a typical length,

$$L_d(t) = \sqrt{2\kappa t}. \tag{10}$$

The smallest (and oldest) structures present in the flow, i.e., those corresponding to the Batchelor wave number, will be given by the crossover point where $L_d \approx L_s$, as shown in Fig. 10.

We take the stretching time τ_s to be the circulation time of a large eddy or the measured correlation time, roughly 4 s for our flow. The dye injection scale is $L_0 = 2.5$ cm. The point of intersection occurs at about 20 s, which gives an estimate of the age of the oldest striations. At that point, $L(t) \approx 0.014$ cm, where

$$\frac{k_B}{2\pi} \cong \frac{1}{2L_{\mathrm{B}}} \approx 35\ \ \mathrm{cm}^{-1}. \tag{11}$$

It should be noted that this model for k_B is fairly insensitive to the characteristic stretching time, the most uncertain parameter used. Increasing τ_s by a factor of 5 only reduces the estimated k_B by a factor of 2. We note that this estimate for k_B is roughly consistent with that obtained from k_c for the regular array according to the relation $k_B=(Sc)^{1/2}k_K$.

Alternately, we can estimate k_B by measuring the mean value of the most negative principal strain rate γ. To do this, we have determined the rate of strain tensor on a regular grid (obtaining the velocity derivatives from our velocity field measurements). We then diagonalize this tensor at each location and ensemble average over space and time. In this way, we estimate that $\gamma \approx 1.0\ s^{-1}$. Using Eq. (6) and defining k_B as the wave number for which the exponent is -1, we find that $k_B=70\ cm^{-1}$, a value that is comparable to but somewhat larger than the estimate given above. Note that the estimates made in this section do not consider the role of strong intermittency, which we discuss in Sec. V.

B. Scalar measurements

1. Concentration fields

We present characteristic data from runs with the regular magnet array and the random magnet arrangement. Water and dye solution were injected in a ratio of 7.5 parts water to

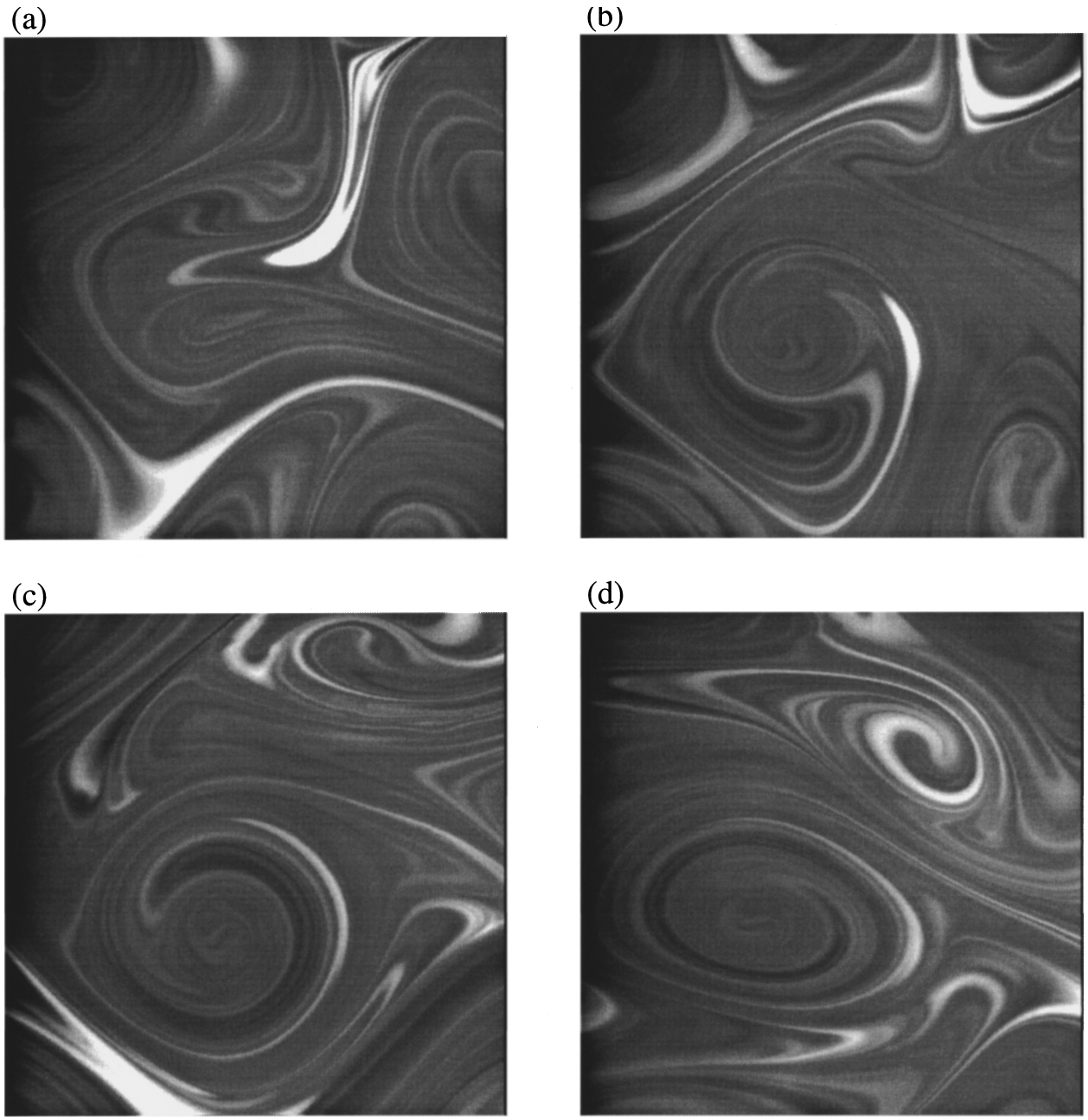

FIG. 11. Sample images of the concentration field during mixing, for the regular magnet array of Fig. 2(a). Bright areas correspond to high concentration. An 8 cm×6.8 cm region is shown at 5 s intervals.

1 part dye solution (by volume). The size of the sponges for dye and water [Fig. 1(b)] sets the injection scale at about 2.5 cm. Due to the sharp edges of the dye distribution upon injection, high-frequency components were also present. For the regular case, the camera imaged a region 4.9 cm square with a corresponding pixel size of 0.0096 cm. Forty-two images were captured over a 210 s period. For the random case the camera was moved farther away to give a pixel size of 0.0200 cm. Fifty-four images were obtained over a 270 s run. The camera exposure was set to 1/66 s for the first run, and 1/45 s for the second. This exposure time was a compromise between blurring and the signal to noise level. In the regions of maximum velocity, the blurring was about three pixels. This proved not to be a limitation as the signal at corresponding wave numbers was less than the noise level. Many other runs in addition to those described here were also done.

Sample images of the concentration fields are shown in Figs. 11 and 12 for the ordered and random magnet arrays. The patterns reveal the stretching and folding characteristic of turbulent or chaotic mixing; the vortices in the underlying velocity field are also evident, but of course the concentration field reflects the time history of the velocity field. The thinnest resolvable features in the images are 1 mm or less in width. However, thinner striations are visible to the eye.

2. Existence of a steady state

The assumption that the distribution of the dye is statistically steady is crucial to the theoretical predictions. Fluc-

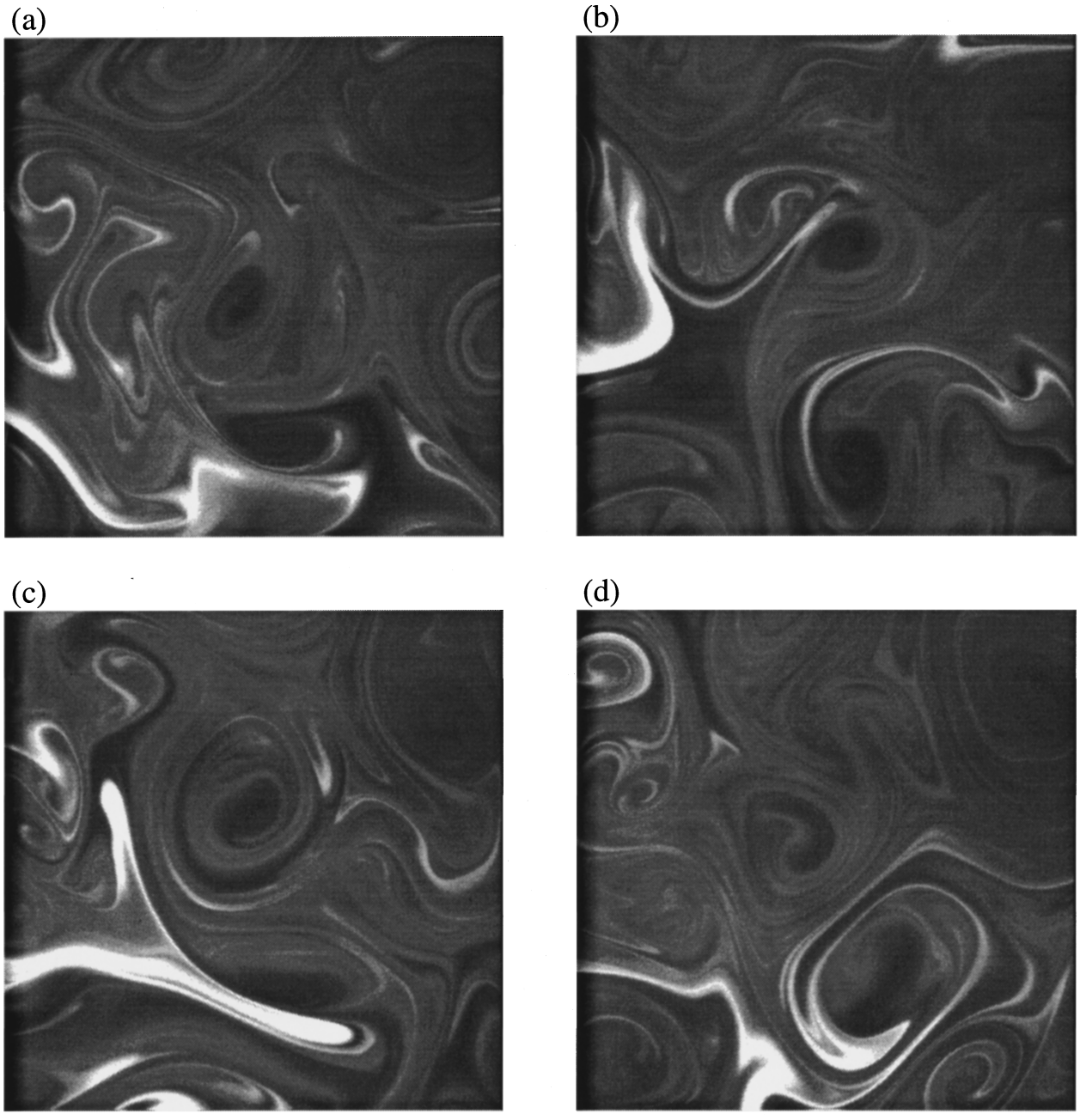

FIG. 12. Sample images of the concentration field during mixing, for the random magnet array of Fig. 2(b). A 10.2×10.2 cm region is shown at 5 s intervals.

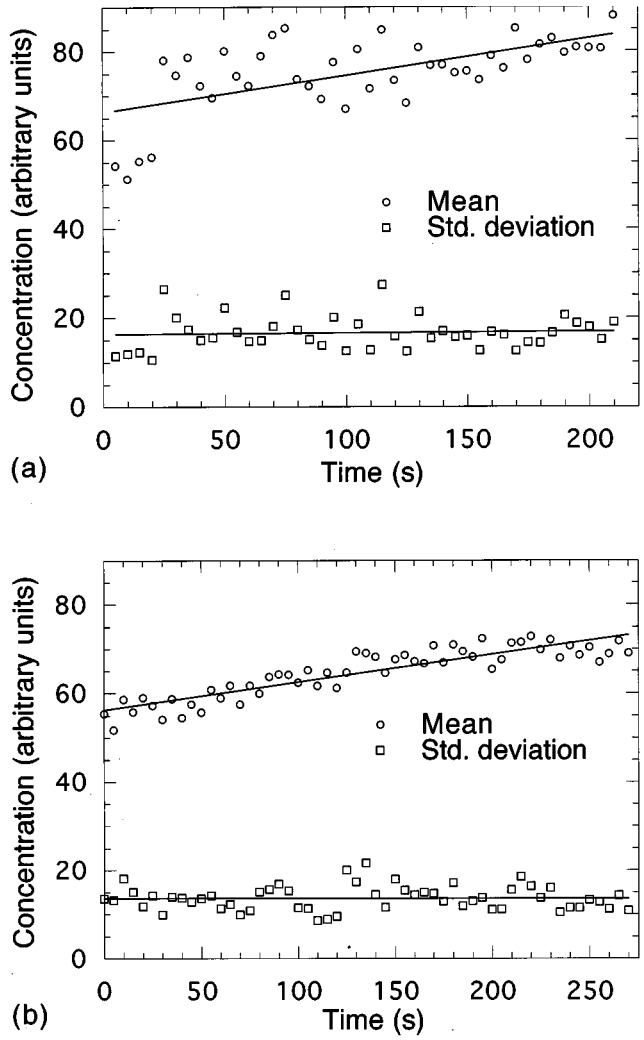

FIG. 13. Mean concentration and standard deviation of concentration fluctuations in the imaged area over time for two types of forcing: (a) regular magnet array and (b) random arrangement. Though the mean concentration drifts upward, the standard deviation is relatively constant.

tuations injected into the flow mainly at low k, are transformed to higher k by advection and stretching, and finally destroyed near k_B. However, the total variance should remain constant over time [Eq. (4)]. The validity of these assumptions for our flow is checked by examining the behavior of the mean dye concentration and its standard deviation over time (Fig. 13). We average the pixel values in each frame to obtain the mean concentration of the imaged area. The lower dataset in each plot is the square root of the spatial variance of the light intensity as a function of time. Since only a small portion of the mixing cell is imaged, and the majority of dye in the cell is outside the camera's view, these values are expected to fluctuate somewhat, but without long term drift. Linear fits approximate the temporal behavior adequately.

We find that the average dye concentration gradually increases over the course of the run. This indicates that the concentration is not in a true steady state; there is a buildup of dye. However, the standard deviation (the lower curves in Fig. 13) increases only slightly with time. We conclude that

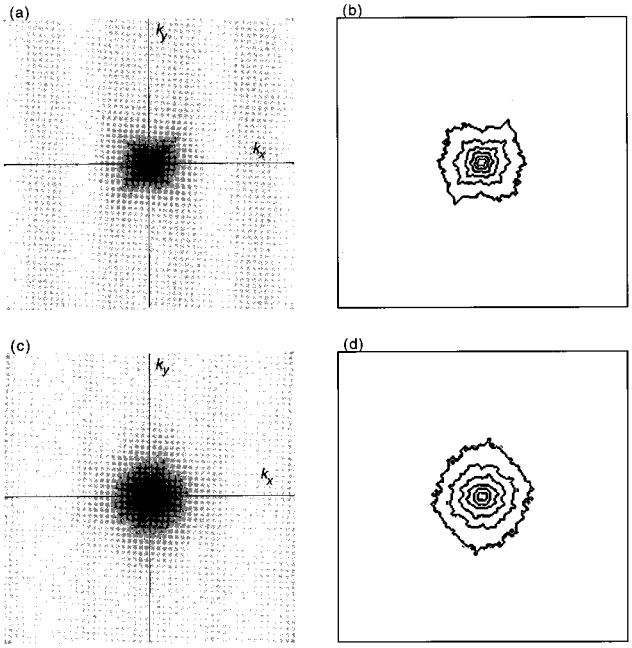

FIG. 14. Characteristic two-dimensional logarithmic power spectrum and contour plot from the run with (a,b) regular magnet array, (c,d) random magnet arrangement.

fluctuations are sufficiently steady for a meaningful measurement of steady-state scalar spectra.

3. Concentration spectra

Two-dimensional spectra $\Delta(\mathbf{k})$ from runs using the regular magnet array and the random arrangement are shown in Fig. 14. The most noticeable characteristic is the broad peak centered at the origin in $\mathbf{k}$ space. One can replace $\Delta(\mathbf{k})$ by the one-dimensional spectral function $E_\theta(k)$, as in Eq. (3), without loss of information, if $\Delta(\mathbf{k})$ is statistically isotropic for the wave numbers of interest. The contour plots in Figs. 14(b) and 14(d) show that the random forcing case is essentially isotropic, while the concentration fluctuations produced by the regular array are less so. This is shown quantitatively in Fig. 15, where the angular dependence of the spectral power,

$$g(\phi)=\int_{k/2\pi=1}^{k/2\pi=10} k\Delta(k,\phi)dk, \tag{12}$$

is plotted for $0<\phi<\pi$. The integral is normalized by the total spectral power in the expected viscous-convective range $1<k/2\pi<10\ \mathrm{cm}^{-1}$. The total power varies with angle by roughly a factor of 2 for regular forcing, but the angular dependence is only marginally detectable for the random array. (With additional ensemble averaging, we believe that the angular fluctuations would decrease further.)

The form of the spectrum is not significantly dependent on angle, even for the regular array, though the amplitude varies somewhat. This fact is demonstrated in Fig. 16, which shows the radial spectra $k\Delta(k,45°)$, and $k\Delta(k,90°)$, taken along the angles of greatest relative anisotropy of the spectrum shown in Figs. 13(a) and 13(b). At both angles, the spectrum is considerably steeper than the Batchelor predic-

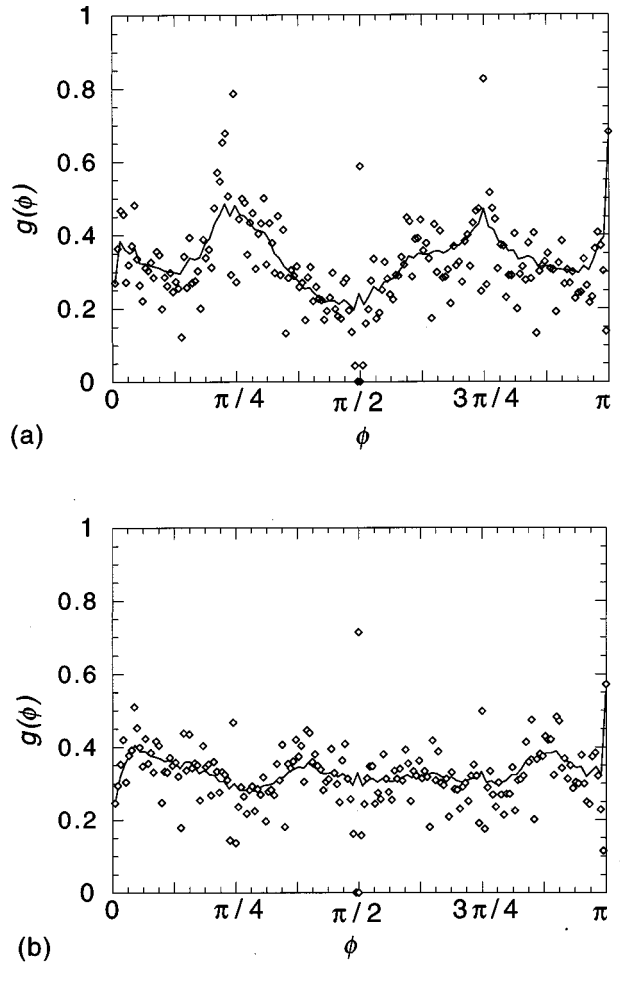

FIG. 15. Angular dependence $g(\phi)$ of the spectral power defined in Eq. (12) for (a) regular forcing and (b) random forcing. The plots are normalized to the unit total area. The solid line is a smoothed fit to the data to guide the eye. The angular dependence is barely detectable for the random case.

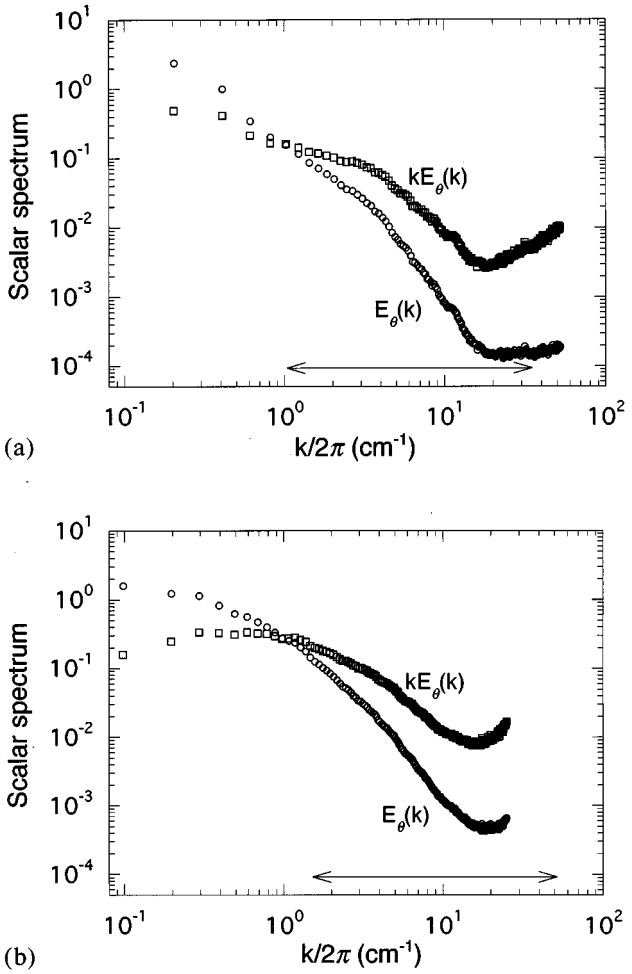

FIG. 17. One-dimensional concentration spectra (normalized by the variance) for two magnet arrangements: (a) regular and (b) random. Also displayed are the compensated spectra $kE_\theta(k)$ that would appear flat for k^{-1} scaling. The estimated viscous-convective range is indicated by an arrow. The structure for wave numbers greater than $k/2\pi = 15\ \mathrm{cm}^{-1}$ in (a) and $k/2\pi = 10\ \mathrm{cm}^{-1}$ in (b) is obscured by noise.

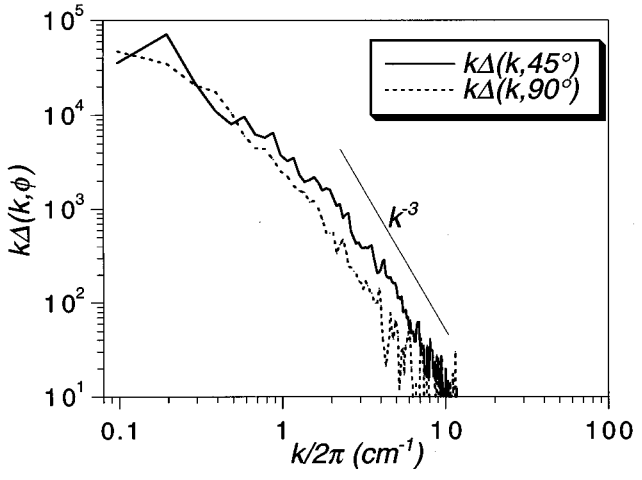

FIG. 16. Radial concentration spectra $k\Delta(k,\phi)$ along 45° and 90° angles, the directions of greatest relative anisotropy for the spectrum shown in Figs. 13(a) and 13(b). The line k^{-3} is drawn only for comparison and is not meant to imply that the function is a power law. The two spectra differ approximately by a constant factor.

tion in the relevant range of wave numbers above $1\ \mathrm{cm}^{-1}$. The two curves differ mainly in amplitude, not shape, so it is acceptable to average the concentration spectrum over angles, even for the regular array.

The one-dimensional spectra $E_\theta(k)$ from both runs are presented in Fig. 17. They are normalized by $\langle(\delta\theta)^2\rangle$ so that the total spectral power is equal to unity. Also shown is the compensated spectrum $kE_\theta(k)$, which should be flat in the Batchelor range. A noise floor (see Appendix A) is reached at approximately $k/2\pi \approx 10-20\ \mathrm{cm}^{-1}$, well below the Nyquist wave number k_N associated with the pixel size. (For the ordered case, $k_N/2\pi = 25\ \mathrm{cm}^{-1}$. For the random case, $k_N/2\pi = 52\ \mathrm{cm}^{-1}$.) Data below $10-20\ \mathrm{cm}^{-1}$ should therefore be ignored.

Nearly a decade of the estimated viscous-convective range (shown by the arrow) is seen in the concentration spectra in both cases. *Note that the uncertainty in the location of this range is about a factor of 2 in wave number*. To examine the spectra in greater detail, we present the logarithmic slopes in Fig. 18. The *slope* generally becomes more nega-

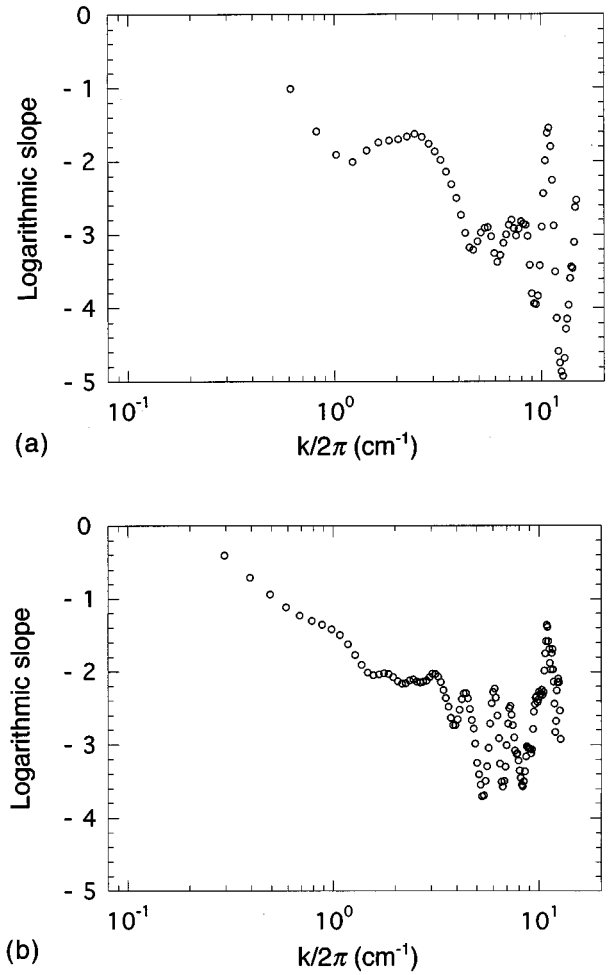

FIG. 18. Logarithmic slopes of concentration spectra displayed in Fig. 17. The slope is less than -1 and is generally decreasing with increasing k.

tive with increasing k, and no well-defined power law behavior is evident. Though regions not too far from k^{-1} scaling occur for a narrow interval near the velocity cutoff k_c, no extended interval of this type occurs. Recall that due to measurement noise, the slope data beyond $k/2\pi = 10-20\ \mathrm{cm}^{-1}$ should be ignored. Many other runs (not shown) are consistent with these results showing an early cutoff.

4. Scalar probability distribution

Additional insight can be gained from examining the probability distribution $P(\delta\theta)$ of the scalar field about its mean; this quantity is shown for the random array in Fig. 19, using the original scale of the digitized intensities (0–255). We estimate that noise broadens any feature slightly by at least 6 in the units shown. The asymmetry of the distribution is due to the fact that more water than dye was injected. The distribution has a roughly Gaussian central peak with extended tails. The small peaks in the tails are related to unmixed components, which are not very prominent. Thus, there is quite a lot of mixed fluid. (This is a time average

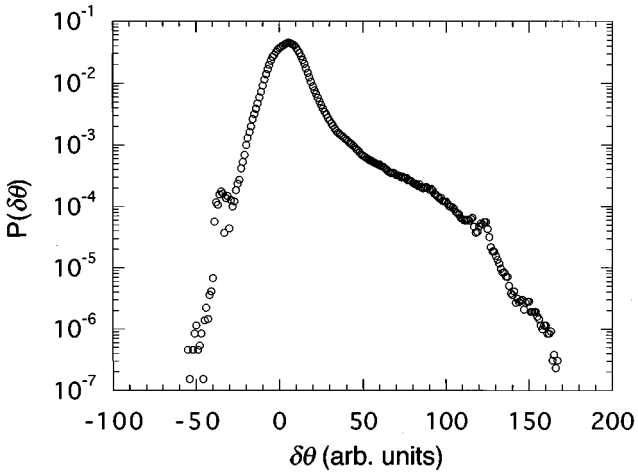

FIG. 19. Probability distribution $P(\delta\theta)$ of the scalar field for the random array. The units correspond to the eight bit intensity digitization, and are the same as in Fig. 13(b). The asymmetry is due to the fact that more water than dye solution was injected. The small peaks in the tails are related to the injected unmixed dye soluiton and pure water.

over the run; the mixed fluid of course builds up during the run.) The ''unmixedness parameter'' proposed by Dimotakis and Miller,[11]

$$\Xi \equiv \frac{\langle (\delta\theta)^2 \rangle}{\langle \theta \rangle (\Delta\theta - \langle \theta \rangle)}, \tag{13}$$

is approximately 0.17. Therefore, we are apparently not very close to the ''binary'' regime where diffusion is unimportant, and only the unmixed components determine the statistics.

5. Time-dependent forcing at higher viscosity

We also studied dye mixing in a rather different flow field produced by a time-periodic (rather than steady) driving current. In this case a somewhat more viscous glycerol–water mixture ($\nu = 3.3$ cS) was utilized that does not easily produce turbulence for steady forcing. The driving current was applied as a square wave with a period of 4 s.

The resulting concentration patterns are shown in Fig. 20. In this case, there are no stable coherent vortices advected about the cell. Rather, the patterns are typical of chaotic advection induced by periodic modulation (for example, see Ref. 20), though the patterns are more irregular than usual due to the random magnet array. The scalar field is stretched and folded efficiently, and very thin dye filaments are visible over a somewhat larger fraction of the flow than in the cases discussed earlier in the paper. However, there is evidence of ''KAM surfaces'' that inhibit mixing; these bound the darker low concentration regions in Fig. 20. As a result, not all paths are equally accessible to fluid elements. An extensive study of the velocity field for this case has not been performed. We use it mainly to see whether the scalar spectra are substantially affected by changing the mixing mechanism. The higher viscosity used in this case also favors two-dimensionality (by reducing vertical gradients of horizontal velocity) to some extent.

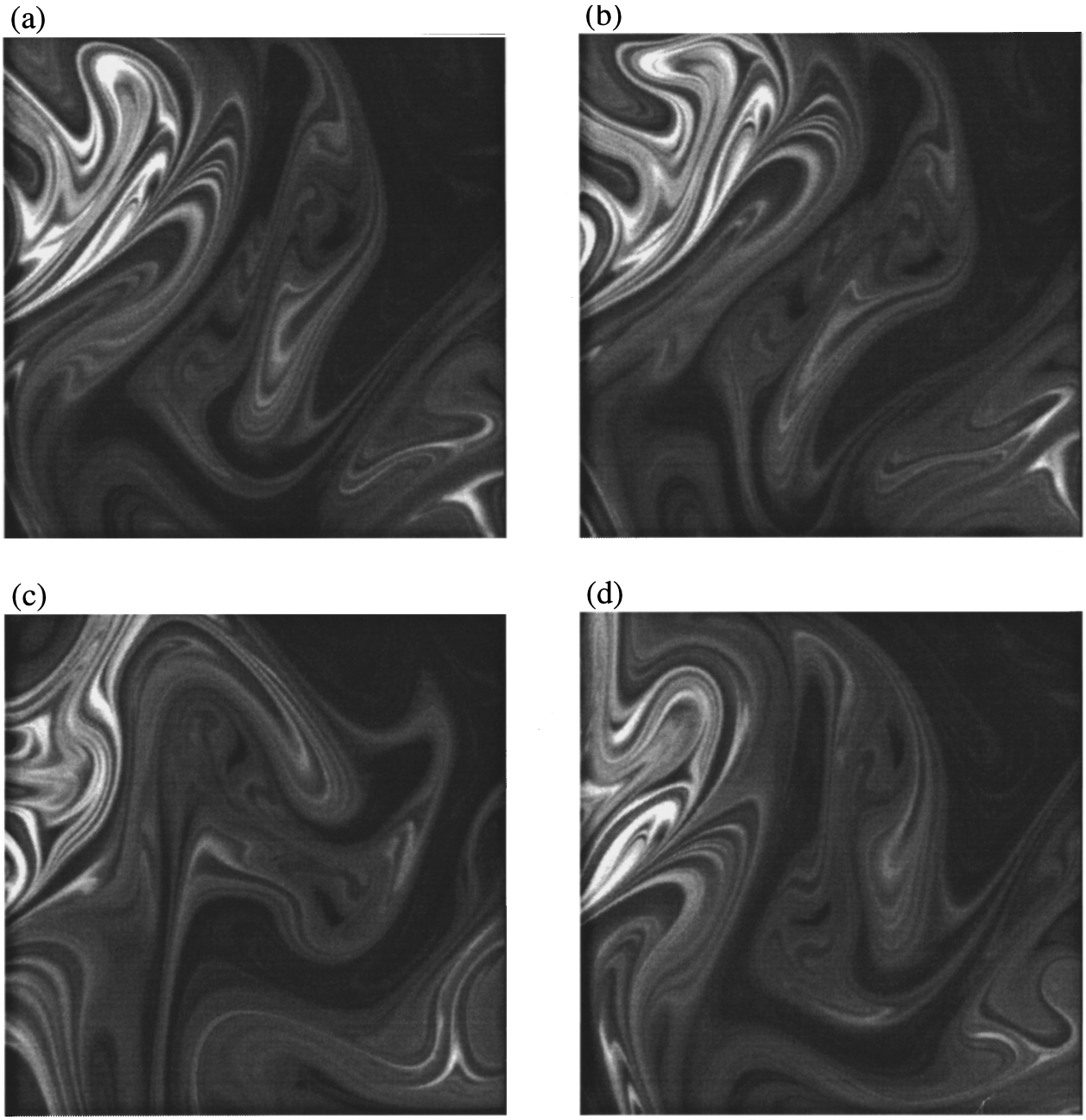

FIG. 20. Images of the concentration fields for time-periodic forcing with the random magnet array, at higher viscosity. These lack coherent vortices and resemble chaotic advection (see the text). A 10.2×10.2 cm region is shown at 5 s intervals.

The one-dimensional power spectrum (Fig. 21) obtained during these runs shows a steep dependence on wave number similar to that observed for steady forcing at lower viscosity, despite the quite different flow. Again, there is no well-defined scaling law.

5. Variation of injection parameters

It is important to determine whether the form of the concentration spectrum is affected by variations of the ''injection'' process. For example, it seemed possible that the spectra are dominated by contributions from highly concentrated dye streamers that emerge directly into the flow from the injection sponges. Examples of such streamers can be seen in Fig. 11. To determine whether these streamers are problematic, a baffle was placed between the injection sponges and the imaged area in some runs, including the one corresponding to the spectrum of Fig. 17(a). In order to enter the flow, dyed fluid and pure water were forced to flow around the edges of the baffle, and thus become more thoroughly mixed before being imaged. Though the presence of the baffle seems to have minor effects on the spectra, it does not substantially affect the steep slope in the major part of the viscous-convective regime.

Since the probability distribution indicated that a substantial amount of mixed fluid accumulates during the runs, we also tried increasing the injection rates by a factor of 3; this did not produce a significant change in the form of the scalar spectrum. *Reducing* the injection rates by a factor of 5

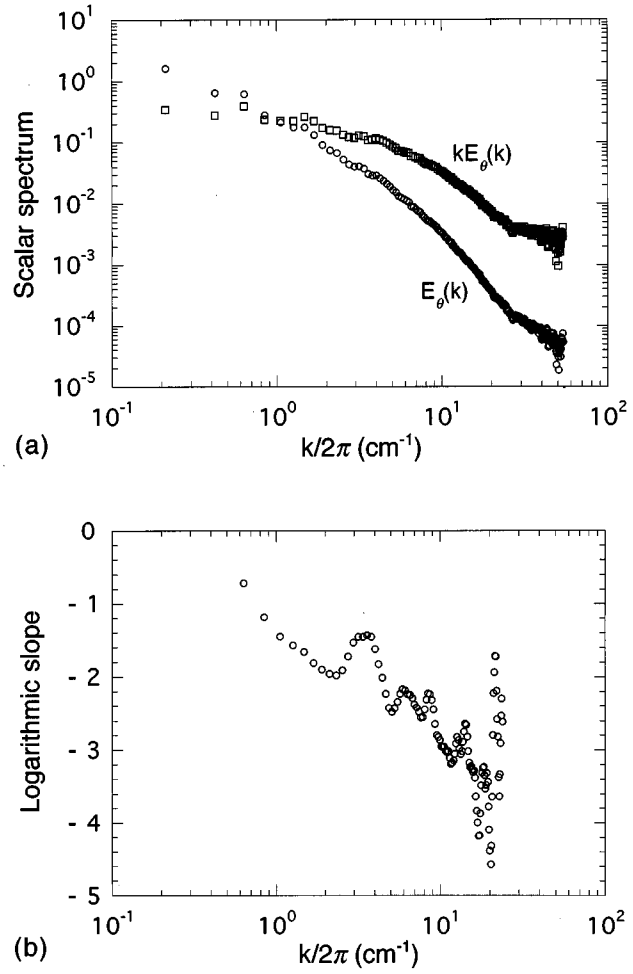

FIG. 21. (a) Normalized one-dimensional concentration spectrum $E_\theta(k)$ and compensated spectrum $kE_\theta(k)$ for the case of periodic forcing of the random magnet array. (b) Logarithmic slope.

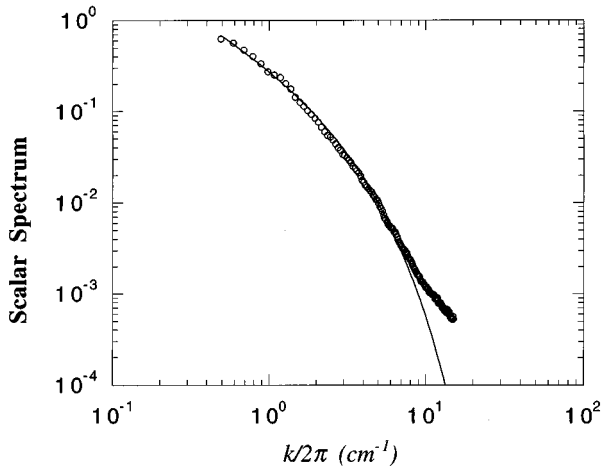

FIG. 22. One-dimensional concentration spectrum of Fig. 17(b), fitted to Eq. (14) (solid line). The inclusion of an exponential tail provides a good fit, but the resulting effective principal strain rate is lower than expected.

from the usual conditions also produced little change in the scalar spectrum. Larger reductions were impractical due to signal-to-noise considerations.

V. CONCLUSION

A. Summary

We have studied the mixing of a dye in quasi-two-dimensional turbulence through examination of the time-averaged spatial power spectrum (Fig. 17) of the dye concentration. We are satisfied that several assumptions essential to the development of the theory of high Schmidt number mixing hold for this experiment. The velocity field is known to be stationary, and its fluctuations were measured to be essentially homogeneous in space and isotropic (Fig. 7). Although there is a mean flow caused by the forcing (Fig. 6), its characteristic length scale is much larger than any of the relevant scales. The establishment of a steady state for the scalar variance was confirmed by monitoring the level of spatial fluctuations over time (Fig. 13). Some anisotropy in the dye distribution is present for the regular magnet array, but there is no detectable angular dependence of the form of the spectrum (Fig. 16). The random array yields essentially isotropic mixing [Fig. 15(b)]. We have considered whether the injection parameters influence the spectrum, and these effects appear to be small. Finally, the emitted light intensity of the dye was found to be proportional to concentration for the range of concentrations and illumination intensities actually used.

We find that the logarithmic spectral slope (Fig. 18) is steeper than -1, except possibly near k_c. Furthermore, the magnitude of the slope increases with k throughout the accessible range. Including a Gaussian tail as in Eq. (6) does not resolve the problem; the fit is very poor. On the other hand, the inclusion of a phenomenological exponential (rather than Gaussian) diffusive tail does yield a satisfactory fit, but requires unphysical parameters. For example, fitting the data shown in Fig. 17(b) to a spectrum of the form

$$E_\theta(k) = Ck^{-1} \exp(-k\sqrt{\kappa/|\gamma_{\text{eff}}|}), \tag{14}$$

yields the result shown in Fig. 22. (Of course, a constant of order 1 could be inserted in the exponent.) Using the physical diffusivity, we find that the effective principal strain rate is $|\gamma_{\text{eff}}| = 1.1 \times 10^{-3}\ \text{s}^{-1}$, much smaller than the *measured* mean strain rate of about $1\ \text{s}^{-1}$. Equivalently, the falloff below k^{-1} scaling occurs at wave numbers lower than expected by approximately a factor of 30.

B. Interpretation

How then we are to understand the surprising experimental results reported here? The key lies largely in the strong intermittency of these two-dimensional flows. Semistable vortices can form and move about the cell, remaining coherent for up to 20 s before being stretched apart. As a result, fluid elements typically experience long quiescent intervals punctuated by infrequent large straining events. During the quiescent intervals the scalar structure may be dissipated at a lower wave number because of the long time available for diffusion to act in the absence of stretching and compression. The chaotic data of Figs. 20, 21 are also affected by intermittency (localized regions of high strain rate), though for somewhat different reasons. Though vortices are

apparently absent in this case, persistent visible barriers to transport are present, so that the flow is not statistically homogeneous.

The effects of intermittency on scalar spectra have been discussed theoretically.[12,15] A recent theoretical approach by Antonsen *et al.* applicable to chaotic mixing[21] predicts that the effects of intermittency may be fairly dramatic. These authors describe the spectrum in terms of a superposition of time-dependent variances associated with Lagrangian fluid elements in a chaotic two-dimensional flow. If the straining motion experienced by a typical fluid element is confined to short bursts separated by long quiescent (nonstretching) intervals of mean length T, then their approach predicts that the cutoff in the scalar spectrum is *reduced* approximately by $\sqrt{\tau_s/T}$, where $\tau_s \approx \gamma^{-1}$ is the mean stretching time defined near Eq. (9). Kraichnan's approach would lead to a similar conclusion: the low strain rate regions, if they predominate statistically, lead to a cutoff lower in wave number than that otherwise expected from the high strain rate regions by roughly the square root of the reduction in strain rate.

We have made preliminary measurements of the probability distribution of the most negative principal strain rate γ from our velocity fields, as explained in Sec. IV A 3. We have established that the strain rates accounting for the highest and lowest deciles of the distribution differ by a factor of *at least* 10, and possibly much more. We cannot make a more precise statement because differentiating the velocity fields augments the effect of measurement noise. We find by numerical tests that a measurement uncertainty of even 2% in the velocity field is problematic for assessing the width of the strain rate distribution quantitatively.

Intermittency is probably not be sufficient to entirely account for the early spectral falloff. However, its effect may be magnified by a small amount of three-dimensionality. These effects are discussed in Appendix B, where we point out that small velocity gradients across the upper layer can tilt the planes of constant concentration away from the vertical. This effect is overwhelmed where random straining is large, since planes of constant concentration align normal to the (horizontal) axis of greatest compression. On the other hand, in the low strain rate regions, significant blurring of sharp structures by about 1–2 mm (somewhat larger than the smallest resolved scales in the spectra) can occur due to residual vertical gradients of the horizontal velocity. This effect, which may contribute to the early spectral falloff, could be made less important by substantially increasing the system size. We note that increasing the viscosity by a factor of 3 as described in Sec. IV B 4, a change that should favor two-dimensionality, did not change the spectra significantly.

C. Concluding remarks

It is tempting to speculate that intermittency (highly nonuniform strain rates) may also have played a role in the interesting jet flow measurements of Miller and Dimotakis,[4] where spectra systematically steeper than k^{-1} were found. The specific form of the falloff found in the present work does not match the lognormal behavior noted by these authors, but this difference is not necessarily a counterargument since the flows are so different. It would be interesting to measure the probability distribution of the most negative principal strain rate for the jet flow, but such measurements may be impractical. Another possible explanation is that a remarkably wide separation between the velocity cutoff and the diffusive cutoff may be needed to obtain convincing k^{-1} scaling in some situations, as found in Pierrehumbert's simulations.[10]

The early pioneering measurements, for example those of Gibson and Schwarz[2] and Nye and Brodkey,[5] contributed much to the subject but also suffered from limited instrumental resolution at high wave number. While these experiments revealed a rough k^{-1} regime (generally below k_c) over a limited range of wave numbers, an early instrumental falloff was observed. Therefore, it was impossible to determine the actual shape and cutoff wave number of the scalar field in its dissipative regime. Whether the extent of the k^{-1} range is as great in these studies as is expected from the theory is unknown.

Disparate conclusions about scalar spectra in the Batchelor regime are prevalent in the literature. This fact probably reflects a greater sensitivity to flow statistics than is sometimes assumed. The results of the present investigation suggest the importance of intermittency, and the delicacy of applying the theory to two-dimensional flows at low Reynolds number. The results also emphasize the difficulty of interpreting scalar spectra without extensive diagnostics on the velocity field. It seems evident that somewhat more than ''random straining'' is required to produce convincing scaling of the type that Batchelor first discussed for weakly diffusing impurities.

ACKNOWLEDGMENTS

E. Siggia first stimulated our interest in this problem. He and B. Shraiman provided many important suggestions along the way. We thank T. Antonsen and E. Ott for helpful discussions of the possible role of intermittency. We also acknowledge helpful discussions with P. Dimotakis, A. Fairhall, W. Goldburg, P. R. Kramer, I. Procaccia, K. R. Sreenivasan, P. Tabeling, and E. Villermaux. Arshad Kudrolli contributed to some of the experiments and provided good advice. T. Sheaffer computed the strain rate distribution from measured velocity fields. B. Boyes built the flow cell. This work was supported by National Science Foundation Grant No. CTS-9115005 and later by Grant No. DMR-9319973. Computational facilities were provided by a grant from the Zimmer Foundation. We also appreciate support provided by a NATO collaborative research grant.

APPENDIX A: SIGNAL PROCESSING

The dye concentration function we wish to study is $\theta(\mathbf{x},t)$. The actual visible radiated light is proportional to the UV light intensity at each point, $I(\mathbf{x})$. The total signal that reaches the CCD array is $\theta(\mathbf{x},t)I(\mathbf{x})$, since we know by a separate calibration run that the dye response is linear. The CCD array has a spatially nonuniform response $r_{\mathrm{CCD}}(\mathbf{x})$. We combine the two into a single response function $r(\mathbf{x}) = I(\mathbf{x})r_{\mathrm{CCD}}(\mathbf{x})$. However, over the range of relevant wave

numbers, spatial variations of the UV lighting and nonuniformities in the CCD sensitivity are expected to be negligible. Therefore we have approximated the response function $r(\mathbf{x})$ as unity.

The CCD has fixed pattern noise, $d(\mathbf{x})$, which we assume to be constant in time. We also include a random noise term $n(\mathbf{x},t)$, due to amplifier noise and fluctuations in the dark current. Therefore the raw received signal, $S_{\text{raw}}(\mathbf{x},t)$, is given by

$$S_{\text{raw}}(\mathbf{x},t)=\theta(\mathbf{x},t)+d(\mathbf{x})+n(\mathbf{x},t). \tag{A1}$$

The fixed pattern noise term $d(\mathbf{x})$ is obtained by taking a series of pictures with the shutter closed for the same integration time. These dark images are averaged together and subtracted from each captured image $S_{\text{raw}}(\mathbf{x},t)$.

Subtracting the fixed pattern noise yields the corrected concentration function plus a noise term:

$$s(\mathbf{x},t)=s_{\text{raw}}(\mathbf{x},t)-d(\mathbf{x})=\theta(\mathbf{x},t)+n(\mathbf{x},t). \tag{A2}$$

This signal $s(\mathbf{x},t)$ is then Fourier transformed. The effect of the Fourier transform is to change $s(\mathbf{x},t)$ to $S(\mathbf{k},t)$ and $\theta(\mathbf{x},t)$ to $\Theta(\mathbf{k},t)$. The noise term $n(\mathbf{x},t)$ becomes $N(\mathbf{k},t)$. We then obtain the power spectrum by taking the complex square of the transform:

$$|S(\mathbf{k},t)|^2=|\Theta(\mathbf{k},t)|^2+|N(\mathbf{k},t)|^2+N(\mathbf{k},t)\Theta(\mathbf{k},t)^*+\Theta(\mathbf{k},t)N(\mathbf{k},t)^*. \tag{A3}$$

The last two terms are the Fourier transforms of the cross-correlation function between $n(\mathbf{x},t)$ and $\theta(\mathbf{x},t)$. Let us suppose for the moment that the noise and the concentration distribution are uncorrelated so these terms vanish. The time-averaged two-dimensional concentration spectrum $\Delta(\mathbf{k})$ can then be obtained by subtracting the noise spectrum from the signal spectrum:

$$\Delta(\mathbf{k})=\langle|\Theta(\mathbf{k},t)|^2\rangle_t=\langle|S(\mathbf{k},t)|^2\rangle_t-\langle|N(\mathbf{k},t)|^2\rangle_t. \tag{A4}$$

This two-dimensional spectrum $\Delta(\mathbf{k})$ can then be used to obtain the one-dimensional spectral function:

$$E_\theta(k)=2\pi k\Delta(k)=\int_0^{2\pi}\Delta(k,\phi)k\,d\phi. \tag{A5}$$

Though the process described here does significantly reduce the spectral background (mainly by eliminating noise associated with the dark current and the amplifier), a noise floor remains in the spectra of Figs. 15, 18, because of additional noise (e.g., shot noise) that is correlated with the signal itself. We believe it is best not to try to remove it.

We have not considered the spatial frequency response of the CCD array and lens. There is actually some attenuation of striations that are narrower than two or three pixels; we do not bother to correct for this effect because our spectra become buried in noise at wave numbers this high.

APPENDIX B: TWO-DIMENSIONALITY OF THE EXPERIMENTAL FLOW

To study mixing, we create a quasi-two-dimensional flow using the methods described in Sec. III A. Though two-dimensionality is not necessary for the Batchelor theory, it is needed to allow imaging measurements. We require that the dye mix only within the 1 mm thick upper layer of pure water, and that the concentration of the dye be uniform over the depth of the layer.

There are two principal ways two-dimensionality could be lost. First, diffusion can reduce the density contrast between the two layers until overturning occurs due to convective secondary flows in the (lower) forcing layer. The diffusivity of NaCl in water is $D=1.484\times10^{-5}\ \text{cm}^2\,\text{s}^{-1}$. The characteristic diffusion length in time t is $L=\sqrt{Dt}$. For an experimental run of 5 min, $L=0.67$ mm, less than the depth of the upper layer. This estimate indicates that it is reasonable to expect the upper layer to remain significantly less dense than the lower layer. The continuous injection of pure water and dye solution and the extraction of mixed fluid also maintains the density gradient. The volume of fluid contained in the upper layer is cycled through the cell once every 4–5 min, roughly the duration of the run. The glass windows in the side of the mixing cell permit inspection of the layers of water and dye. It is evident to the eye that the two layers remain separate for the duration of the run.

A second way that two-dimensionality can be lost is through the development of vertical gradients of horizontal velocity in the upper layer. If the dye at the upper and lower portions of the layer move at different speeds in a direction perpendicular to isoconcentration planes, thin structures of dye will become tilted with respect to the vertical, and will appear to the camera less intense and thicker than they actually are.

The major source of such velocity gradients is the acceleration associated with the rotation of vortices, for the steady forcing experiments. This effect may be assessed as follows. Suppose that a vortex of radius r rotates at angular velocity ω. The pressure difference from the center to outer edge of the vortex that is needed to sustain this motion is approximately $\rho\omega^2r^2/2$. The fractional head (thickness variation) $\Delta h/h$ required to provide this pressure difference is $v^2/2gh=0.01$ typically. The time τ required for such small thickness variations to develop is quite short: $\tau=(2r/v)(\Delta h/h)\approx0.05$ s. This means that in the steady-state *spinout of fluid is strongly suppressed* and that one need not depend primarily on viscosity to limit vertical gradients of velocity. However, during the *transient* periods of sudden acceleration, one can get displacements across the layer of about $\nu\tau\approx0.05$ cm, a value sufficiently small not to be a major concern.

However, small residual pressure variations tend to give weak secondary flows (outward at the upper edge of a vortex and inward at its lower edge). These are hard to estimate *a priori*, but their effect on the scalar field is suppressed by the random straining process described by Batchelor.[1] Planes of constant scalar concentration tend to become aligned along the axis of greatest strain, with their normals along the direction of maximum compression. This effect increases the wave number of dye components during advection. Since the velocity gradients are much larger in the horizontal directions, the principal axis of greatest contraction will also be horizontal. Therefore, planes of constant concentration will tend to remain vertical. This effect opposes the formation of

three-dimensional structure in the scalar field.

In regions of the flow where straining motion predominates, evidence of two-dimensionality is supported by direct observation of the flow. Dye filaments are observed to be approximately 0.1 mm wide, much smaller than the depth of the upper layer; they are aligned vertically. However, inside the vortices, which can remain coherent for times much longer than the eddy turnover time, some smearing occurs over distances of 1–2 mm, somewhat larger than the smallest scale resolved in the spectrum. Thus, the combination of intermittency with this weak smearing effect may contribute to the early spectral falloff.

[1]G. K. Batchelor, ''Small-scale variation of convected quantities like temperature in a turbulent field. Part 1. General discussion and the case of small conductivity,'' J. Fluid Mech. **5**, 113 (1959).

[2]C. H. Gibson and W. H. Schwarz, ''The universal equilibrium spectra of turbulent velocity and scalar fields,'' J. Fluid. Mech. **16**, 365 (1963).

[3]H. L. Grant, B. A. Hughes, W. M. Vogel, and A. Moilliet, ''The spectrum of temperature fluctuations in turbulent flow,'' J. Fluid. Mech. **34**, 423 (1968).

[4]P. L. Miller and P. E. Dimotakis, ''Measurements of scalar power spectra in high Schmidt number turbulent jets,'' J. Fluid. Mech. **308**, 129 (1996).

[5]J. O. Nye and R. S. Brodkey, ''The scalar spectrum in the viscous-convective subrange,'' J. Fluid. Mech. **29**, 151 (1967).

[6]X.-L. Wu, B. Martin, H. Kellay, and W. I. Goldburg, ''Hydrodynamic convection in a two-dimensional couette cell,'' Phys. Rev. Lett. **75**, 236 (1995).

[7]M. Holzer and E. D. Siggia, ''Turbulent mixing of a passive scalar,'' Phys. Fluids **6**, 1820 (1994).

[8]D. Bogucki, J. A. Domaradzki, and P. K. Yeung, ''Direct numerical simulations of passive scalars with Pr>1 advected by turbulent flow,'' to appear in J. Fluid Mech.

[9]T. M. Antonsen, F. F. Fan, and E. Ott, ''*k* spectrum of passive scalars in Lagrangian chaotic fluid flows,'' Phys. Rev. Lett. **75**, 1751 (1995).

[10]R. T. Pierrehumbert, ''Tracer microstructure in the large-eddy dominated regime,'' Chaos Solitons Fract. **4**, 1091 (1993).

[11]P. E. Dimotakis and P. L. Miller, ''Some consequences of the boundedness of scalar fluctuations,'' Phys. Fluids A **2**, 1919 (1990).

[12]R. H. Kraichnan, ''Small-scale structure of a scalar field convected by turbulence,'' Phys. Fluids **11**, 945 (1968).

[13]A. Vulpiani, ''Lagrangian chaos and small scale structure of passive scalars,'' Physica D **38**, 372 (1989).

[14]A. Gargett, ''Evolution of scalar spectra with the decay of turbulence in a stratified fluid,'' J. Fluid. Mech. **159**, 379 (1985).

[15]C. H. Gibson, ''Kolmogorov similarity hypotheses for scalar fields: Sampling intermittent turbulent mixing in the ocean and galaxy,'' Proc. R. Soc. London Ser. A **434**, 149 (1991).

[16]P. L. Miller and P. E. Dimotakis, ''Reynolds number dependence of scalar fluctuations in a high Schmidt number turbulent jet,'' Phys. Fluids A **3**, 1156 (1991).

[17]O. Cardoso, D. Marteau, and P. Tabeling, ''Quantitative experimental study of the free decay of quasi-two-dimensional turbulence,'' Phys. Rev. E **49**, 454 (1994).

[18]B. J. Gluckman, H. Willaime, and J. P. Gollub, ''Geometry of isothermal and isoconcentration surfaces in thermal turbulence,'' Phys. Fluids A **5**, 647 (1992).

[19]C. E. Willert and M. Gharib, ''Digital particle image velocimetry,'' Exp. Fluids **10**, 181 (1991).

[20]J. M. Ottino, ''Mixing, chaotic advection, and turbulence,'' Annu. Rev. Fluid Mech. **22**, 207 (1990).

[21]T. M. Antonsen, Z. Fan, E. Ott, and E. Garcia-Lopez, ''The role of chaotic orbits in the determination of power spectra of passive scalars,'' Phys. Fluids (in press).